

UNCLASSIFIED

AD NUMBER
AD846913
NEW LIMITATION CHANGE
TO Approved for public release, distribution unlimited
FROM Distribution authorized to U.S. Gov't. agencies and their contractors; Critical Technology; Aug 1968. Other requests shall be referred to US Naval Ordnance Lab., White Oak, Silver Spring, MD.
AUTHORITY
Naval Ordnance Lab ltr, 15 Nov 1971

THIS PAGE IS UNCLASSIFIED

AD 846913

FOR THE RECORDS OF THE HOUSE OF REPRESENTATIVES
COMMITTEE ON THE BUDGET
WASHINGTON, D. C.

BY AUTHORITY OF THE HOUSE OF REPRESENTATIVES

PRINTED AT THE GPO: 1964 O - 350-000

THIS REPORT IS AVAILABLE FOR SALE BY THE GPO
AT A SPECIAL PRICE OF \$1.00 PER COPY
FOR INFORMATION OF THE PUBLIC

ON HYPERSONIC BLUNT BODY FLOW FIELDS OBTAINED WITH A
TIME-DEPENDENT TECHNIQUE

Prepared by:
John D. Anderson, Jr.
Lorenzo M. Albacete
Allen E. Winkelmann

ABSTRACT: New results are presented for inviscid, supersonic and hypersonic blunt-body flow fields obtained with a numerical time-dependent method patterned after that of Moretti and Abbett. In addition, important comments are made with regard to the physical and numerical nature of the method. Specifically, numerical results are presented for two-dimensional and axisymmetric parabolic and cubic blunt bodies as well as blunted wedges and cones; these results are presented for zero degrees angle of attack and for a calorically perfect gas with $\gamma = 1.4$. The numerical results are compared with other existing theoretical and experimental data. Also, the effects of initial conditions and boundary conditions are systematically examined with regard to the convergence of the time-dependent numerical solutions, and the point is made that the initial conditions can not be completely arbitrary. Finally, in order to learn more about the performance of the time-dependent method, a numerical experiment is conducted to examine the unsteady propagation and region of influence of a slight pressure disturbance introduced at a point on the surface of a blunt body.

U. S. NAVAL ORDNANCE LABORATORY
WHITE OAK, MARYLAND

21 August 1968

ON HYPERSONIC BLUNT-BODY FLOW FIELDS OBTAINED WITH A
TIME-DEPENDENT TECHNIQUE

This report presents new results for inviscid, calorically perfect, supersonic and hypersonic blunt-body flow fields obtained with a time-dependent numerical method. In addition, important comments are made with regard to the physical and numerical nature of the method.

This work was performed under the support of the Independent Exploratory Development (IED) Program (Problem 043). In addition, the authors wish to acknowledge helpful discussions with Dr. E. I. Harris and Mr. Robert H. Feldhuhn of the Aerophysics Division (AOL), and with Dr. W. L. Melnik of the University of Maryland during the course of the analysis.

E. F. SCHREITER
Captain, USN
Commander

L. H. Schindel
L. H. SCHINDEL
By direction

CONTENTS

	Page
INTRODUCTION.....	1
ANALYSIS.....	3
Basic Equations and Transformations.....	3
Inner Points and Finite Differences.....	4
Shock, Body Points, and Characteristics.....	5
RESULTS.....	6
Two-Dimensional Flow-Field Results.....	7
On the Propagation of a Weak-Pressure Disturbance.....	10
Experiments on the Sensitivity of the Blunt-Body Solution to Initial Conditions, Body Shape, and Boundary Conditions.....	11
Axisymmetric Flow-Field Results.....	13
CONCLUSIONS.....	16
REFERENCES.....	18

ILLUSTRATIONS

Figure	Title
1	Coordinate System
2	Time Variation of Wave Velocity; Parabolic Cylinder; $M_\infty = 4$
3	Time Variation of Stagnation-Point Pressure; Parabolic Cylinder; $M_\infty = 4$
4	Time Dependent Shock-Wave Motion; Parabolic Cylinder; $M_\infty = 4$
5	Surface Pressure Distributions; Parabolic Cylinder
6	Shock Shapes and Sonic Lines; Parabolic Cylinder
7	Velocity Direction Field; Parabolic Cylinder; $M_\infty = 4$
8	Time Variation of Stagnation-Point Pressure; Parabolic Cylinder; $M_\infty = 8$
9	Time-Dependent Shock-Wave Motion; Cubic Cylinder, $M_\infty = 4$
10	Surface-Pressure Distribution; Cubic Cylinder, $M_\infty = 4$
11	Time Variation of Stagnation-Point Pressure; Blunted Wedge, $M_\infty = 8$
12	Time-Dependent Shock-Wave Motion; Blunted Wedge; $M_\infty = 8$
13	Surface-Pressure Distribution; Blunted Wedge; $M_\infty = 8$
14	Sonic-Line Time Variation; Blunted Wedge; $M_\infty = 8$
15	Velocity Variation Along Stagnation Streamline
16	Configuration for Protuberance Experiment
17	Disturbed Surface-Pressure Variations
18	Disturbed Surface-Pressure Variations, Cont.
19	Centerline Wave Velocity with and without Disturbance
20	Time Variation of Wave Velocity; Paraboloid; $M_\infty = 4$
21	Time Variation of Wave Velocity; Paraboloid; $M_\infty = 8$

ILLUSTRATIONS (CON'T)

- 22 Time Variation of Stagnation-Point Pressure; Paraboloid;
 $M_\infty = 4$
- 23 Time Variation of Stagnation-Point Pressure; Paraboloid;
 $M_\infty = 8$
- 24 Time Dependent Shock-Wave Motion; Paraboloid; $M_\infty = 4$
- 25 Time Dependent Shock-Wave Motion; Paraboloid; $M_\infty = 8$
- 26 Surface-Pressure Distribution; Paraboloid; $M_\infty = 4$
- 27 Surface-Pressure Distribution; Paraboloid; $M_\infty = 6$
- 28 Surface-Pressure Distribution; Sphere-Cone, $M_\infty = 4$
- 29 Surface-Pressure Distribution; Sphere-Cone, $M_\infty = 8$
- 30 Surface-Pressure Distribution; (Expanded Scale) Sphere-
Cone, $M_\infty = 4$
- 31 Surface-Pressure Distribution; (Expanded Scale) Sphere-
Cone, $M_\infty = 8$
- 32 Shock-Wave Shapes; Sphere-Cone
- 33 Shock-Wave Shape and Sonic Line; Sphere-Cone; $M_\infty = 4$
- 34 Shock-Wave Shape and Sonic Line; Sphere-Cone; $M_\infty = 8$
- 35 Velocity Distribution; Sphere-Cone; $M_\infty = 4$
- 36 Velocity Distribution; Sphere-Cone; $M_\infty = 8$
- 37 Velocity Variation Along Stagnation Streamline; Paraboloid
- 38 Velocity Variation Along Stagnation Streamline; Sphere-Cone
- 39 Sonic Line; Paraboloid; $M_\infty = 4$
- 40 Effect of Extrapolation to Upper Boundary on Pressure
Distribution; Paraboloid; $M_\infty = 4$

LIST OF SYMBOLS

a	speed of sound
b	abscissa of the body in the x, y plane
g	dummy variable
L	characteristic length
M	Mach number
p	pressure (divided by free-stream pressure)
P	$\ln p$
r	radius of cylinder, sphere, or paraboloid
R	$\ln \rho$
s	abscissa of the shock of the x, y plane; also distance along surface of the body
t	nondimensional time in physical coordinate system
T	nondimensional time in transformed coordinate system
u	nondimensional velocity in x direction in x, y plane
v	nondimensional velocity in y direction in x, y plane
W	velocity of the shock in x direction in x, y plane
x	abscissa in a Cartesian frame in the physical plane
y	ordinate in a Cartesian frame in the physical plane
Y	ordinate in a Cartesian frame in the transformed plane
ξ, η	Cartesian reference frame along shock or body
δ	s - b
γ	ratio of specific heats
ρ	density (divided by free-stream density)
θ	angle between tangent to shock and x axis
ζ	abscissa in a Cartesian reference frame in the transformed plane
\ddagger	$\ln p - \ln \rho$

The subscript ∞ indicates, as usual, free-stream conditions.

ON HYPERSONIC BLUNT-BODY FLOW FIELDS OBTAINED WITH A
TIME-DEPENDENT TECHNIQUE

by

John D. Anderson, Jr.
Lorenzo M. Albacete
Allen F. WinkelmannINTRODUCTION

Experimental and analytical investigations of supersonic and hypersonic flow fields about blunt bodies have been prevalent in aerodynamic research for the past two decades. This is in part due to the practical use of blunt bodies for manned and unmanned re-entry vehicles, as well as to the intellectually challenging mathematical nature of the mixed subsonic-supersonic flow field which is characteristic of such bodies. However, as pointed out in reference (1), it is remarkable that the present state-of-the-art has still not progressed to the point where one specific analytical technique for solving the blunt-body problem can be agreed upon as being markedly superior to all others. On the other hand, a relatively new technique has appeared in the recent literature which appears to have the potential for such pre-eminence among inviscid blunt-body solutions; namely, the time-dependent approach such as employed by Bohachevsky et al (refs. (2) and (3)), and more recently by Moretti and Abbett (ref. (4)), and Moretti and Blich (ref. (5)). The present report supplements the above investigations by further examination and application of the time-dependent method to various two-dimensional and axisymmetric blunt bodies.

It is not within the scope of the present report to give a detailed review of the various analytical approaches to the blunt-body problem; indeed, excellent descriptions of the significant theories are readily available in the literature. (For example, see references (1), (6), and (7).) Instead, it is sufficient and pertinent to describe briefly the philosophy of the time-dependent method, after which the specific purposes of the present report will be outlined.

The time-dependent blunt-body approach entails the solution of the unsteady partial differential equations which physically describe the transient flow field; i.e., the equations contain time derivatives of the local flow properties. Given a fixed body shape and free-stream conditions, the solution begins by assuming (somewhat, but not completely) arbitrary initial values for the flow field variables and shock-wave shape and location. The solution then proceeds, using the unsteady equations, to obtain new values of the flow field variables and shock-wave shape in steps of time. This solution is carried out numerically by a finite-difference scheme using a high-speed digital computer. Following a natural relaxation process, the solution asymptotically approaches a

steady state for large values of time. For the present investigation, this steady state is the desired result; the use of the time-dependent equations is just a means to an end. However, the transient numerical variation of the flow field variables during their approach to the steady state should approximate the actual physical relaxation associated with a flow which is artificially started with the assumed initial conditions. (How well this transient process is approximated depends on how well the time-dependent difference equations approximate the original governing partial differential equations.) Therefore, the time-dependent approach is also useful for the analyses of inherently transient problems; for example, the establishment of flow about models in a shock tube, and the interaction of a blast wave with a re-entry vehicle (ref. (8)). Nevertheless, from the point of view of the steady supersonic blunt-body problem, the mathematical advantage obtained by use of the time-dependent method is that the partial differential equations are hyperbolic in time; this is in contrast to the steady flow equations which are elliptic in the subsonic region and hyperbolic in the supersonic region. This hyperbolic nature of the time-dependent solution allows the use of a finite-difference approach starting with assumed initial conditions at a given time. A considerably more detailed description of the time-dependent method can be found in references (2) to (5), and therefore, no further elaboration will be given here. However, for the purposes of establishing nomenclature and for making this report somewhat self-contained, the pertinent equations and numerical solution employed in the present investigation will be outlined in a subsequent section.

The present report gives new results for blunt-body flow fields obtained with a time-dependent method patterned after that of Moretti and Abbett (ref. (4)), and also makes some important comments with regard to the physical and numerical nature of the method. Specifically, the main purposes of the present report are fourfold:

- (1) To document numerical results for two-dimensional and axisymmetric, supersonic and hypersonic flow fields about various blunt body shapes; namely analytical shapes (parabolic and cubic) as well as blunted wedges and blunted cones. Results are presented for zero degrees angle of attack and for a calorically perfect gas with $\gamma = 1.4$.
- (2) To compare numerical results with other existing theoretical and experimental data.
- (3) To systematically describe the effects of different assumed initial conditions and differently obtained boundary conditions on the convergence of the time-dependent numerical solutions.
- (4) To describe the results of a numerical experiment conducted to answer the following question: If a slight pressure disturbance is introduced at a point in the supersonic portion of the blunt-body flow field, what is its region of influence and how clearly is it defined by the time-dependent analysis employed in the present investigation? The answer to this question has significance with regard to the type of body configuration which can be realistically treated by the above analysis.

ANALYSIS

Basic Equations and Transformations

Since our method of solution is patterned after Moretti and Abbott's analysis, described in reference (4), we give here only a synopsis of the procedure, intended primarily to permit discussion of our results. The reader is thus referred to reference (4) for the details.

We are considering the inviscid flow around a body, as shown in figure 1a. The body BC (either two-dimensional or axisymmetric) is assumed symmetric with respect to the x axis; AD is an arc of the unknown shock wave; the location of C is such that the flow is always supersonic along CD; the flow at infinity is uniform, supersonic, and parallel to the x axis.

The governing equations are:

$$\text{Continuity} \quad \frac{\partial \rho}{\partial t} + \frac{\partial}{\partial x} (\rho u) + \frac{\partial}{\partial y} (\rho v) + K \frac{\rho v}{y} = 0 \quad (1)$$

$$\text{x Momentum} \quad \rho \frac{\partial u}{\partial t} + \rho u \frac{\partial u}{\partial x} + \rho v \frac{\partial u}{\partial y} = - \frac{\partial p}{\partial x} \quad (2)$$

$$\text{y Momentum} \quad \rho \frac{\partial v}{\partial t} + \rho u \frac{\partial v}{\partial x} + \rho v \frac{\partial v}{\partial y} = - \frac{\partial p}{\partial y} \quad (3)$$

$$\text{Energy} \quad \frac{\partial \dot{\phi}}{\partial t} + u \frac{\partial \dot{\phi}}{\partial x} + v \frac{\partial \dot{\phi}}{\partial y} = 0 \quad (4)$$

In equation (1), $K = 0$ for the two-dimensional configuration, and $K = 1$ for the axisymmetric case. In equation (4), $\dot{\phi} = \ln p - \gamma \ln \rho$. The energy equation thus corresponds to

$$\frac{D\dot{\phi}}{Dt} = 0 = \frac{D}{Dt} \left(\frac{P}{\rho^\gamma} \right)$$

for a calorically perfect gas. The additional symbolism is summarized in the list of symbols at the beginning of this report.

$$\zeta = \frac{x-b}{\delta}, \quad y = y; \quad T = t \quad (5)$$

where $\delta = s-b$, the local shock detachment distance. The definitions (5) transform the "oblique" region of interest ABCD into a rectangular region, as shown in figure 1b.

In addition, the following variables are defined:

$$\begin{aligned} C &= (\zeta - 1) \frac{db}{dy} - \zeta \cot \theta \\ P &= \ln p \\ R &= \ln \rho \\ B &= [U - W\zeta + vC] / \delta \end{aligned} \quad (6)$$

where W is the velocity of the shock wave.

All the variables are non-dimensionalized as follows: p and ρ are divided by their free-stream values; the velocities are divided by $[p_\infty/\rho_\infty]^{1/2}$; the lengths are divided by a characteristic length L ; and thus the non-dimensional time is the dimensional time divided by $L/\sqrt{p_\infty/\rho_\infty}$.

All of these operations result in the following non-dimensional, transformed equations:

$$\text{Continuity} \quad \frac{\partial R}{\partial T} = - \left[B \frac{\partial R}{\partial \zeta} + \frac{1}{\zeta} \frac{\partial u}{\partial \zeta} + \frac{C}{\delta} \frac{\partial v}{\partial \zeta} + \frac{\partial v}{\partial y} + v \frac{\partial R}{\partial y} + K \frac{v}{y} \right] \quad (7)$$

$$\text{x Momentum} \quad \frac{\partial u}{\partial T} = - \left[B \frac{\partial u}{\partial \zeta} + v \frac{\partial u}{\partial y} + \frac{p}{\rho \delta} \frac{\partial p}{\partial \zeta} \right] \quad (8)$$

$$\text{y Momentum} \quad \frac{\partial v}{\partial T} = - \left[B \frac{\partial v}{\partial \zeta} + v \frac{\partial v}{\partial y} + \frac{\rho C}{\rho \delta} \frac{\partial p}{\partial \zeta} + \frac{p}{\rho} \frac{\partial p}{\partial y} \right] \quad (9)$$

$$\text{Energy} \quad \frac{\partial \xi}{\partial T} = - \left[B \frac{\partial \xi}{\partial \zeta} + v \frac{\partial \xi}{\partial y} \right] \quad (10)$$

Now, in the spirit of reference (4), the flow field is divided into three parts: The shock itself (AD), the body (BC), and the "inner points" inside the rectangle ABCD.

Inner Points and Finite Differences

We consider first the inner points. As indicated in the introduction, the use of the unsteady equations (hyperbolic in time) enables us to employ a finite-difference approach starting from the initial conditions at an initial time. The particular finite-difference form is a matter of choice. In this analysis, after Moretti and Abbett, we use, for any flow variable g :

$$g(T + \Delta T) = g(T) + \frac{\partial g}{\partial T}(T) \cdot \Delta T + \frac{\partial^2 g}{\partial T^2}(T) \cdot \frac{(\Delta T)^2}{2} \quad (11)$$

That is, given initial conditions for each variable, equation (11) enables us to obtain its value at a later time. These values serve in turn as "initial conditions" for the next time step, and the process continues until the unsteady terms are negligible. This will then be the final solution for the steady problem, approached asymptotically with time.

All the terms in the right-hand side of (11) are known: $\rho(T)$ is known from the previous time step and the first time derivatives are given by the governing equations (7) and (10). In these equations, the space derivatives are computed by central finite-differences at each point in a mesh which subdivides the inner region. The second time derivatives are obtained by differentiating equations (7) through (10). Symmetry is assumed at the centerline for the calculation of the space derivatives.

For the axisymmetric case, there will be indeterminate terms at the centerline of the form 0/0. These may be calculated by the use of L'Hospital rule.

In these calculations, the step size ΔT is evaluated as the minimum of $\Delta/1.5 a$ and $(M+1)$ where Δ is the smallest interval between Δy and Δx , a is the speed of sound, and M the Mach number. This satisfies the Courant-Friedrichs-Lewy stability criterion.

Finally, note that in obtaining the second time derivatives by differentiating equations (7) to (10), the term $\frac{\partial B}{\partial T}$ will be encountered. From equation (6) this implies that $\frac{\partial W}{\partial T}$ must be known. This term is computed as follows:

$$\frac{\partial W}{\partial T} = \left[W(T + \Delta T) - W(T) \right] / \Delta T \quad (12)$$

This means that every time the inner points are calculated, the value of $W(T+\Delta T)$, (that is the "new" value of W), must be known. For this reason, the shock points must be computed first, before the interior points, at the beginning of each step in time.

Shock, Body Points, and Characteristics

The values of the flow variables behind the shock at $T + \Delta T$ can be obtained from the Rankine-Hugoniot relations for a moving shock. But this means that a value for $W(T+\Delta T)$ must be assumed, since it is not known at the beginning of each step in the computation. However, the values for the shock points can be obtained in another way, compared to those obtained from the shock relations with the assumed W , and matched by an iterative process until they do agree. This will give the true value of $W(T+\Delta T)$ as well as the rest of the unknowns. In the analysis of Moretti and Abbett, this "other way" is by means of the characteristic equations for the set of governing relations written for a (ξ, η, t) frame, where ξ and η are Cartesian coordinates normal and tangential to the shock respectively. The assumption is made in obtaining the characteristics that the governing equations can be written as quasi-one-dimensional, modified by "forcing terms" containing derivatives in the tangential direction. That is, the characteristics are found in the (ξ, t) plane. For the axisymmetric case, the same assumptions are made. However, there exist in the characteristic equation an added "forcing term" arising from the extra term in the continuity equation. This

is $\frac{\partial \tilde{w}}{\partial t}$ where \tilde{w} is the component of the velocity in the w direction perpendicular to the (ξ, η) plane. This term has a value of v/y , as can be determined from geometric considerations. At any rate, the characteristic equation is still quasi-one-dimensional, that is, the characteristics are still found in the (ξ, t) plane. The details of the iteration procedure, the determination of the characteristic lines, and the integration of the compatibility equation, are given in references (4) and (5).

A similar computation is performed at the body. The analysis is simpler, since the body wall is fixed.

Finally, the values for the points on the upper boundary are extrapolated linearly from the inner values.

All the points in the flow field are thus accounted for.

RESULTS

In general, the following results serve to complement those of Moretti and Abbett (ref. (4)), and also lead to significant comments with regard to the nature and practical use of the time-dependent approach of reference (4). In addition, interesting comparisons are made with existing theoretical and empirical results, including the useful correlations by Billig (ref. (9)) for shock-wave shape and detachment distance. In particular, flow-field results have been obtained for the following blunt bodies at zero degrees angle of attack:

(1) Parabolic cylinder at $M_\infty = 4$ and 8, with the cross section given by

$$b = 0.769 y^2 - 1.0$$

(2) Cubic cylinder at $M_\infty = 4$, with the cross section given by

$$b = 0.427 y^3 - 1.0$$

(3) Blunted wedge at $M_\infty = 8$, consisting of a cylindrical nose of unit radius, a transition section, and a wedge at an angle of 14 degrees with the horizontal. As explained later, the small transition section is required to smooth the otherwise discontinuous curvature at the junction point of the circular cylinder and the wedge. This transition section is graphically determined, and its deviation from the purely cylinder-wedge shape is small.

(4) Paraboloid of revolution at $M_\infty = 4$ and 8, with the cross section given by

$$b = 0.769 r^2 - 1.0$$

(5) Sphere cone at $M_\infty = 4$ and 8, consisting of a spherical nose of unit radius, a transition section determined graphically, and a cone afterbody with a 14 degree half-angle.

All of the following results have been obtained for a calorically perfect gas with $\gamma = 1.4$. In addition, the same grid size was used for all the numerical calculations; namely, a rectangle (see figure 1b) with X from 0 to 1 and Y from 0 to 2, with equal increments of $1/7$ along both the X and Y axis respectively.

The results will be given in four sections. First, new results for several two-dimensional blunt-body flow fields will be presented and compared with other available theories. Then, significant results pertaining to the propagation of a pressure disturbance will be shown and interpreted. Next, the latitude within which the initial conditions can be "arbitrarily" assumed will be examined and discussed and the effect of differently obtained boundary conditions will be presented. Finally, the results for the axisymmetric case will be presented and compared with some existing theoretical and experimental data.

Two-Dimensional Flow-Field Results

To begin with, typical paths which the time-dependent solution follows to a steady state are shown in figures 2 and 3 for the case of the parabolic cylinder at $M_\infty = 4$. Figure 2 shows the transient behavior of W on the centerline, and figure 3 shows the time variation of stagnation-point pressure. In both cases, the assumed initial value is the proper steady-state value. Two points are noted from these figures: (1) the most extreme variations occur at early times where the "driving potential" towards the steady state is the strongest, and (2) the steady state is rapidly approached (and for practical purposes, is achieved) at large values of time. In addition to the above results, figure 4 shows the time-dependent shock-wave motion for the parabolic cylinder at $M_\infty = 4$. Again, the rapid approach to a steady state is obvious. After about 300 time steps, the final shock shape and location are well defined. (The steady-state results presented in this report are those obtained after 500 time steps.) Other indexes are also used to measure the degree to which the steady state is achieved, such as the variation of centerline entropy and position of the sonic line. All of these indexes indicate that the steady state was achieved (practically speaking) for the cases given in the present report.

Final steady-state surface-pressure distributions, normalized with respect to stagnation point pressure, are given in figure 5 for the parabolic cylinder at $M_\infty = 4$ and 8. These results are compared with the modified Newtonian Formula (ref. (10)). Figure 5 contains two anticipated results; namely, that the modified Newtonian distribution underestimates the actual pressure distribution, and that the actual pressure distribution is closer to Newtonian at $M_\infty = 8$ than at $M_\infty = 4$. This type of comparison with modified Newtonian is typical of two-dimensional blunt bodies; in practice, pressure distributions over axisymmetric bodies agree more closely with modified Newtonian than do two-dimensional pressure distributions, as will be shown later.

The fiscal shock shapes and sonic lines are shown in figure 6 for the parabolic cylinder at $M_\infty = 4$ and 8. The decreased shock-detachment distance and downward shift of the sonic line are both characteristic of an increased Mach number. In addition, the resulting shape of the sonic line is proper for two-dimensional blunt bodies at $M_\infty > 2$. (For example, see reference (1).)

Figure 7 shows the steady-state streamline direction field for the parabolic cylinder at $M_\infty = 4$.

Figure 8, which shows the time variation of stagnation point pressure for $M_\infty = 8$, demonstrates a particularly interesting point when compared with figure 3, which is for $M_\infty = 4$. Starting with similar initially assumed flow fields and shock shape, figures 3 and 8 demonstrate that the approach to a steady state is approximately a factor of 4 faster at $M_\infty = 8$ than at $M_\infty = 4$. In fact, for $M_\infty = 8$, $\ln(p_0/p_\infty)$ has converged to within 0.1 percent of its steady-state value by $t = 1.0$; this is in contrast to $t = 4.0$ for similar convergence at $M_\infty = 4$. These results prompt the following explanation. The factor of 4 difference in relaxation time exists because the local sound speed and the local flow velocity within the shock layer are both increased by approximately a factor of two in going from $M_\infty = 4$ to $M_\infty = 8$. Consequently, relative to the fixed body, the velocity of a weak-pressure wave propagating downstream is increased by a factor of 4, resulting in faster relaxation (by a factor of 4) of the flow field to the steady state. The above phenomena identify the following simple gasdynamic mechanism. The rapidly changing unsteady bow shock wave causes transient pressure changes immediately behind the wave. In turn, the subsequent downstream propagation and interaction of these unsteady pressure waves constitute the primary physical mechanism by which the unsteady flow field relaxes to the steady state.

Results obtained for the cubic cylinder at $M_\infty = 4$ are shown in figures 9 and 10, which illustrate the shock-wave shape and surface pressure distribution. Again, the shock-wave shape is seen to rapidly approach a steady state, and as before, the surface pressure distribution is compared with modified Newtonian.

A two-dimensional configuration of more practical importance is that of a blunted wedge; therefore, such results are presented in figures 11-14 for $M_\infty = 8$. As an index of the convergence behavior, figure 11 shows the time variation of stagnation point pressure. Again, the rapid convergence to the steady state is obvious; $\ln(p_0/p_\infty)$ has converged to within 0.1 percent of its steady-state value by $t = 1.0$. And again, the fast relaxation associated with the Mach number is noted. In fact, the approach to the steady state and the relaxation time shown in figure 11 are comparable to those shown in figure 8 for the parabolic cylinder, thus indicating that relaxation time is relatively independent of body shape.

Figure 12 presents the time-dependent bow-shock wave motion, as well as the final shock wave and sonic line. Rapid convergence is also apparent in this figure. In addition, results obtained from the correlation of Billig (ref. (9)) for final shock-wave shape and location are also presented in figure 12. For a cylinder-wedge, the correlation is:

$$\frac{x}{R} = 1 + \frac{\delta}{R} = \left[\left(1 + \frac{y^2 \tan^2 \theta}{R_c^2} \right)^{1/2} - 1 \right] R_c \cot^2 \theta$$

where $\frac{\delta}{R} = 0.386 \exp(4.67/M_\infty^2)$
 and $\frac{R_c}{R} = 1.386 \exp \left[1.8/(M_\infty - 1)^{0.75} \right]$ (13)

δ is the shock detachment distance. R is the cylinder radius, R_c is the shock vertex radius of curvature, and θ is the shock angle approached asymptotically for large y ; in the present case, θ is the attached oblique shock angle for the wedge afterbody. The results presented in figure 12 show very good agreement between Billig's correlation and present exact numerical solution.

The steady-state surface pressure distribution over the blunted wedge as a function of the vertical coordinate, Y , is shown in figure 13. (Also shown is the extent of the transition section mentioned earlier.) Two points are noted from this figure: (1) the proper supersonic wedge pressure is achieved asymptotically and monotonically far downstream of the blunt nose; and (2) the pressure distribution over the cylindrical portion compares favorably with infinite Mach number circular cylinder results obtained by Fuller using an inverse method (refs. (1) and (11)). At hypersonic speeds, the pressure distribution is somewhat insensitive to M_∞ . Consequently, an infinite Mach number comparison is reasonably valid.

Figure 14 illustrates the sensitive transient behavior of the sonic line during convergence to the steady state. Here again two points are of interest: (1) rapid convergence to a steady-state sonic line is obvious, and (2) the movement of the sonic point on the bow shock wave is considerably greater than on the body; in fact, the sonic point movement on the body is confined to a relatively narrow region.

Figure 15 illustrates the steady-state velocity distribution along the stagnation streamline. The results are shown for the parabolic cylinder at $M_\infty = 4$ and 8, the cylinder-wedge at $M_\infty = 8$, and the cubic cylinder at $M_\infty = 8$. The radii of curvature at the stagnation point for these bodies are 0.65, 1 and infinite, respectively. In figure 15, U_1 is the velocity immediately behind the normal portion of the shock, and δ is the shock detachment distance. The fact that the velocity distribution is approximately linear has been noted in previous analyses (ref. (1)). However, the exact nonlinear velocity distributions are identical (within graphical accuracy) for the given two-dimensional cases (but this was not so for the axisymmetric configurations, as will be seen later). Consequently, it appears that for the two-dimensional cases

the exact velocity distribution along the centerline is relatively independent of both Mach number and body shape. Such independence has been predicted by the closed-form approximate analysis of Li and Geiger (ref. (12)). However, the approximate velocity distribution obtained from Li and Geiger's formula differs somewhat from the present numerical results as seen from figure 15.

On the Propagation of a Weak Pressure Disturbance

The following results are given in answer to the question asked earlier in the introduction; namely, if a slight pressure disturbance is introduced at a point in the supersonic portion of the blunt-body flow field, what is its region of influence and how clearly is it defined by the time-dependent analysis employed in the present investigation? Towards this end, a numerical experiment was conducted in which, first, the steady state was reasonably achieved (after 400 time steps) for the flow over the parabolic cylinder at $M_\infty = 4$, and then a small protuberance was extended into the flow from the body surface at a point far downstream of the sonic point, as shown in figure 16. The pressure disturbance caused by this protuberance was subsequently observed as a function of time. Figures 17 and 18 show the time variation of the body surface pressure at the various points identified in figure 16. Note that the scale is the same for all curves shown in figures 17 and 18. Also note that the expanded scale gives the exaggerated illusion of a time varying pressure before the time of the disturbance; in reality, the steady state has been achieved for all practical purposes by this time. These results show that the protuberance indeed causes a noticeable pressure disturbance; this disturbance was strongest at the protuberance, and decays both downstream and upstream of the source. Note also the growing time lag of the disturbance felt at points further away from the protuberance. Of most consequence, however, is the fact that the effect of the protuberance, which is far inside the supersonic region of the flow field, is felt upstream, even to the extent of the subsonic portion of the flow field and all the way to the stagnation streamline. This latter effect is graphically shown in figure 19, which compares the time variations of centerline wave velocity for the cases with and without the disturbance. As seen in this figure, the disturbance is obviously felt all the way to the centerline.

The upstream influence described above, which is contrary to the normal behavior in a steady supersonic flow, can be attributed to the fact that the insertion of the protuberance initiates a new transient flow field (ref. (13)); consequently, all regions of the flow field can eventually be influenced by unsteady wave motion. In addition, even though the disturbed pressures shown in figures 17 and 18 have not settled to a steady state at the largest time considered, the pressures at the upstream locations appear to experience a "permanent set," i.e., the pressures seem to be approaching steady-state values different from the original steady-state values before the disturbance. This "pseudo-elliptic" behavior can be attributed to a numerical effect; namely, the internal wave caused by the disturbance is smeared over several mesh points, and because a coarse grid is employed, the wave can be felt some distance upstream. If at least one of these mesh points is upstream of the sonic point (as in the

present case) then the entire steady-state subsonic region will be affected. The above results have significant practical implication; namely, that the present analysis should be applied to smooth configurations.

It must be emphasized that the present results do not degrade or detract from the excellent and useful method presented in reference (4); quite the contrary, the present authors have already stated their opinion in the introduction that the time-dependent method (such as formulated by Moretti and Abbett) may become pre-eminent among practical blunt-body solutions. Instead, the present results provide some indication that the method (in its present formulation) should be restricted to smooth bodies. Finally, it is interesting to note that the method of reference (4) does indeed sense the presence of a disturbance or internal wave, and such a wave may be traced rather coarsely by means of the peaks in the pressure and density distributions.

Experiments on the Sensitivity of the Blunt-Body Solution to Initial Conditions, Body Shape, and Boundary Conditions

In addition to the above numerical experiment, other experiments were performed to investigate the effect of initial conditions, body shape, and boundary conditions on the time-dependent blunt-body solutions. These experiments indicate that such factors have a definite influence on the "go" or "no-go" nature of the blunt-body computer program. The assumed initial flow field (at time equal to zero) is obtained from the following: (1) modified Newtonian pressure distribution along the body surface, (2) isentropic expansion along the body streamline, (3) assumed shock shape and detachment distance, and (4) linear interpolation between the shock and the body.

a. Effect of Initial Pressure Distribution

Solutions for a two-dimensional parabolic body were obtained using initial pressure distributions which were factors of six above and below the standard solution. In each case, the solution converged to the same final results. From this it is concluded that the program is not very sensitive to initial pressure distributions, which can be prescribed within an order of magnitude of the final pressure distribution.

b. Effect of Shock Shape

Satisfactory results were obtained for a two-dimensional parabolic body using both parabolic and cubic initial shock shapes, with $\delta = .37$ at $M_\infty = 4$. However, the use of a hyperbolic shock shape, $\delta = .37$, did not lead to a converged solution. Hence, the initial shock shape may have some influence on the program, and it appears reasonable to run similar analytic shapes for both the body and the shock. For blunted wedges and cones initial parabolic shock shapes were satisfactory.

c. Effect of Shock-Detachment Distance

The initial shock-detachment distance, δ_{initial} is an important quantity, and can be prescribed only within a certain latitude. For example, using a two-dimensional parabolic body and initial shock shape at $M_{\infty} = 4$ the program worked successfully for $\delta_{\text{initial}} = 0.37$ and 0.49 , but it did not run for $\delta_{\text{initial}} = 0.55$ or 0.20 . Consequently, the initial shock cannot be assumed too close or too far away from the body. If indeed δ_{initial} is too large or too small, the shock wave tends to accelerate considerably faster than shown on figure 2 at early values of time (accelerations an order of magnitude faster can occur). In turn, strong gradients of the flow-field variables are produced behind the highly accelerating wave, and consequently the finite-difference scheme using a fixed course grid becomes inaccurate. This inaccuracy ultimately causes some aspect of the program to collapse.

d. Effect of Body Shape

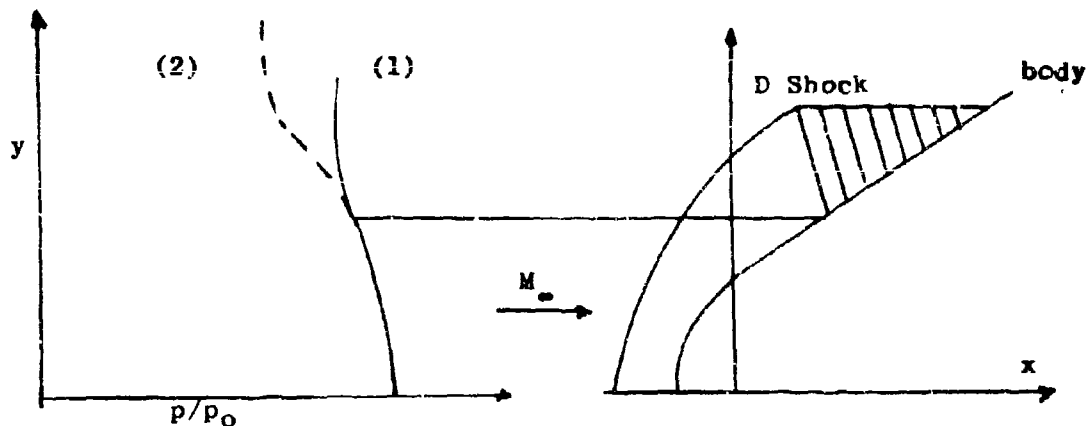
Successful solutions were obtained for bodies with constant and linear variations of d^2b/dy^2 , namely parabolic and cubic shapes, respectively. However, the program did not run for those parabolic and cubic shapes which were characterized by high values of d^2b/dy^2 (above approximately 6). In addition, the program did not run for bodies with local discontinuities in d^2b/dy^2 , namely, purely hemicylinder-wedge or sphere-cone shapes. The program became unstable in the region of the discontinuity in d^2b/dy^2 , i.e., where the body curvature is discontinuous. When a transition section was added to the discontinuity, successful solutions were obtained.

e. Effect of Extrapolation to the Upper Boundary

As shown in figure 1a and as discussed earlier, the upper boundary of the flow field is taken as a horizontal line within the supersonic region. At any given time step, flow-field variables along this boundary are obtained by linear extrapolation from points below. Consequently, the upper boundary values do not exactly satisfy the continuity, momentum and energy equations, and therefore final results for certain portions of the flow field may be compromised. In order to make a preliminary investigation of this effect, results obtained by using several different extrapolation procedures were compared. These extrapolation procedures are:

- (1) linear extrapolation
- (2) reduced linear extrapolation (extrapolated increment reduced 20 percent below that for strictly linear extrapolation)
- (3) Shank's approximation (ref. (14))

We consider first the two-dimensional case. Preliminary data were obtained for a cylinder-wedge in helium ($\gamma = 1.67$) at $M_{\infty} = 16$. These data show that procedures (1) and (2) give different surface pressure results downstream of the right running characteristic from point D, as shown schematically in the diagram below.



Also, procedure (3) resulted in a collapse of the computer program, hence no results were obtained. Obviously, for this case, the procedure for extrapolation to the upper boundary influences that part of the flow field downstream of the right running characteristic from D (shaded region in the above sketch), and this fact should be kept in mind when interpreting the present numerical results. However, this anomalous behavior seems to be limited to the flow field around composite shapes (such as a cylinder-wedge and sphere-cone); the flow field around purely analytical shapes appears to be rather insensitive to the extrapolation procedure, as will be discussed further in a subsequent section dealing with axisymmetric results. A complete resolution and understanding of this effect is deferred for future investigation.

As an interim summary, the convergent or divergent behavior of the time-dependent blunt-body solution appears to be somewhat dependent upon the initial conditions and body shape, outside of a certain latitude. Within this latitude, successful solutions were obtained. However, it should be remembered that a fixed grid size (7x14) was employed for all the present results. A finer grid might reasonably lead to an even wider latitude for successful initial conditions and body shapes. Also, it is apparent that a substantial portion of the supersonic flow field is affected by the extrapolation procedure to the upper boundary.

Axisymmetric Flow Field Results

As for the two-dimensional case, typical paths which the three-dimensional time-dependent solution follows to a steady state are shown in figures 20, 21, 22, and 23. Figures 20 and 21 show the time variation of wave velocity at the centerline for the paraboloid of revolution at $M_\infty = 4$ and 8, respectively. Qualitatively, both figures are similar to the two-dimensional case, in which the most extreme variations occur at early times, but steady state is achieved earlier in the axisymmetric case due to the three-dimensional relieving effect. Figures 22 and 23 show the time variation of the stagnation point pressure for the paraboloid at $M_\infty = 4$ and 8, respectively.

Figures 24 and 25 present the time-dependent shock-wave motion for the paraboloid at $M_\infty = 4$ and 8, respectively. After about 200 time steps, the final shock shape and location are well defined.

In figures 26 and 27 we have plotted the final, steady-state surface pressure distributions (divided by the stagnation point pressure) for the paraboloid at $M_\infty = 4$ and 8, respectively. We can see that the Newtonian pressure distribution is in better agreement with the axisymmetric case than with the two-dimensional case (cf. figure 5). In addition, the pressure distribution is compared with results obtained with the inverse method of Lomax and Inouye (ref. (15)). (All data from this source were kindly provided by Mr. Robert Thompson of the Naval Ship Research and Development Center, Washington, D. C.)

Figures 28 and 29 present results for the sphere-cone case at $M_\infty = 4$ and 8, respectively. We can see again the close agreement between the modified Newtonian distribution and the time-dependent results. These figures also show the overexpansion and subsequent approach to the cone-pressure value, as indicated by P_C/P_O . Note that the abscissa in these figures is "s", the distance along the surface of the body.

In addition, results from reference (16) (which uses a program similar to Lomax and Inouye's, coupled with a method of characteristics (downstream)) are included in figure 29. We see that agreement is good up to $s \sim 0.8$, after which our pressure distribution falls below both the Newtonian distribution and that of reference (16). We believe this to be due to the presence of our transition section, which begins near this point. The exact location of the transition section, and further comparisons with other methods, appear in the next two figures. Figures 30 and 31 present the same results as 28 and 29 but covering a smaller region of the s coordinate shown in an enlarged scale. This was done to facilitate comparison of our results with existing theoretical and experimental data for spheres. In particular, figure 30 compares the present time-dependent calculations for $M_\infty = 4$ with the inverse method of reference (15); the time-dependent results of Moretti and Abbett (ref. (4)), the analytical results of Van Tuyl obtained with rational approximations (ref. (17)), and the experimental data of Stallings (ref. (18)). Good agreement is obtained over most of the spherical portion; however, some effect in the region of the transition section is again noticeable. Figure 31 shows similar results for $M_\infty = 8$.

Figure 32 shows the final shock shapes for the sphere-cone at $M_\infty = 4$ and 8. As in the case of the cylinder-wedge, excellent agreement with the correlation of Billig for the shock shape is obtained for the sphere-cone. In addition, the shock shapes are compared to the ones obtained with the method of reference (15) in figures 33 and 34 for $M_\infty = 4$ and 8, respectively. Once more, excellent agreement is noted.

NOLTR 68-129

A comparison of shock-detachment distance is made with the inverse method of Lomax and Inouye (ref. (15)) in the following table. R is the local radius of curvature at the stagnation point. The agreement is quite good.

Shape	M_∞	δ/R	
		Ref. (15))	Present results
Sphere	4	.1759	.1760
	8	.1396	.1395
Paraboloid $b = 0.769 y^2 - 1.0$	4	.1264	.1284
	8	.098	.100
Paraboloid $b = 0.450 y^2 - 1.0$	8	.1689	.1687

The velocity distributions for the sphere-cone at $M_\infty = 4$ and 8 are given in figures 35 and 36, respectively. The results are compared to Van Tuyl's distributions (ref. (17)) and indeed excellent agreement is observed.

For the axisymmetric case, figures 37 and 38 (which correspond to figure 15 for the two-dimensional case) give the steady-state velocity distribution along the stagnation streamline. Indeed, the velocity distribution is approximately linear as expected, but, unlike the two-dimensional results, the distributions are not exactly independent of Mach number and body shape (although they are close). Once more, the approximate velocity distribution obtained from Li and Geiger's formula (ref. (12)) differs from our numerical results.

Figure 39 compares our sonic line for the $M_\infty = 4$ paraboloid to the sonic line obtained with the method of reference (15). The agreement is excellent. The agreement was not so good, however, for the sphere-cone case, probably because of the presence of the transition section, located indeed in the neighborhood of the sonic point.

Finally, figure 40 illustrates the effect on the surface pressure distribution about a paraboloid at $M_\infty = 4$ of various extrapolation procedures to the upper boundary. We can see that these have little effect. On the other hand, the sphere-cone case is sensitive to the kind of extrapolation procedure used; for example, a converging solution using Shank's approximation could not be obtained. Taken in conjunction with similar results for the two-dimensional case (cf. (e), p. 12), we are led to believe that the flow field around composite shapes (i.e., where there exist discontinuities in the curvature) are particularly sensitive to instabilities. But the flow field around purely analytical shapes does not exhibit this sensitivity.

CONCLUSIONS

New results for calorically perfect, supersonic and hypersonic flow fields about blunt bodies at zero degrees angle of attack have been presented which complement those of Moretti and Abbett (ref. (4)), and which prompt some significant comments with regard to the physical and numerical nature of the present time-dependent method. These results lead to the following conclusions:

(1) Pressure waves which originate behind the initially unsteady, moving bow shock and which subsequently propagate and interact downstream appear to be the principal physical mechanism by which the unsteady flow field converges to the steady state. Consequently, higher free-stream Mach numbers (and thus higher values of the local speed of sound and flow velocities within the flow field) result in proportionally shorter physical convergence times.

(2) A pressure disturbance caused by a protuberance which is suddenly introduced into the steady supersonic region can propagate upstream as well as downstream, and can eventually affect all regions of the flow field. This behavior is a result of the unsteady wave motion and new transient flow field initiated by the disturbance. However, the disturbed upstream surface pressures appear to approach new steady-state values which are displaced from the steady-state values before the disturbance. This apparent "pseudo-elliptic" behavior is attributed to the smearing out of the wave over the rather coarse grid used in the finite-difference scheme.

(3) Billig's empirical correlation for bow shock shape and location agrees very well with the present numerical solutions for cylinder-wedges and sphere-cones.

(4) Whether the numerical solution converges or diverges depends to some extent on the assumed initial conditions. These initial conditions, such as bow shock-wave shape and location, can be arbitrarily assumed within a relatively wide latitude. However, beyond this latitude, the initial conditions do not lead to convergence. Therefore, for practical numerical reasons, the initial conditions can not be completely arbitrary.

(5) Convergent solutions could not be obtained about body shapes with a local discontinuity in the surface curvature. Therefore, the present numerical program is restricted to relatively smooth bodies.

(6) The flow field around composite shapes (such as a cylinder-wedge or sphere-cone) is particularly sensitive to instabilities, whereas the flow field around purely analytical shapes does not exhibit this sensitivity.

Even though some of the above conclusions delineate restrictions on the time-dependent method as employed in the present investigation, emphasis must be made that all existing blunt-body solutions

are restricted in some respect. In comparison with other techniques, the time-dependent method has the advantage of being a direct method (body-shape and free-stream properties are given) as well as being able to calculate large portions of the supersonic flow field downstream of the sonic line (the existing steady-state blunt-body methods usually encounter difficulties in integrating downstream of the sonic line). In addition, the time-dependent method does not involve any simplification or reduction of the equations of change, and in this respect it is an exact solution. Finally, it is anticipated that the time-dependent method will be able to treat more complex body shapes than the existing steady-state methods. For these reasons, and from experience gained during the present investigation, the time-dependent solution appears to have the potential for pre-eminent application to the supersonic and hypersonic blunt-body problem.

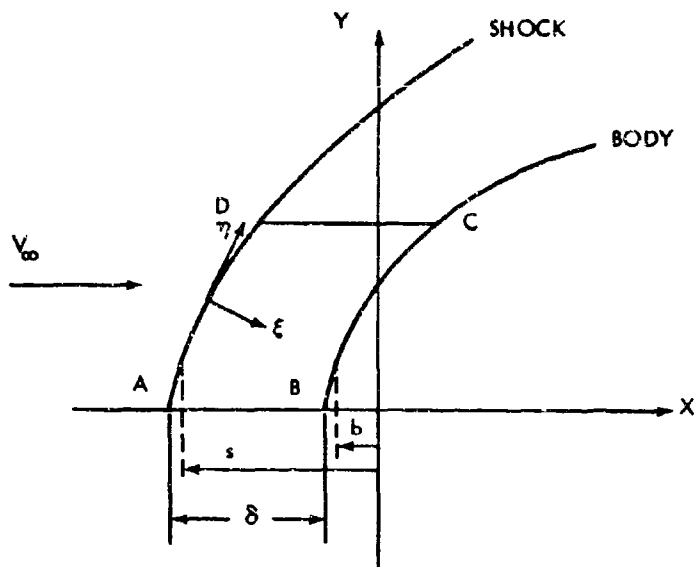
Finally, since the completion of the present studies, additional information concerning the time-dependent blunt-body method has very recently been presented by Moretti (ref. (19)). In general, reference 19 confirms many of the findings of the present studies, and in addition, it presents a large number of blunt-body flow-field calculations in a systematic form for a range of free-stream Mach numbers and body shapes.

REFERENCES

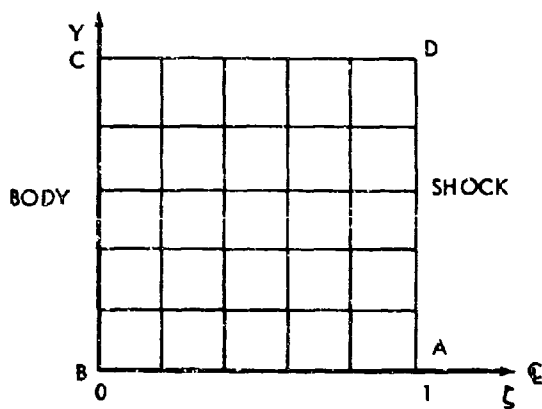
1. Hayes, Wallace D., and Probstein, Ronald F., Hypersonic Flow Theory, Volume I, Inviscid Flows, Academic Press, New York, 1966, Chapter 6
2. Bohachevsky, I. O., and Rubin, E. L., "A Direct Method for Computation of Nonequilibrium Flows with Detached Shock Waves," AIAA Journal, Vol 4, No. 4, Apr. 1966, p 600-6-7
3. Bohachevsky, I. O., and Mates, R. E., "A Direct Method for Calculation of the Flow About an Axisymmetric Blunt Body at Angle of Attack," AIAA Journal, Vol 4, No. 5, May 1966, p 776-782
4. Moretti, G. and Abbett, M., "A Time Dependent Computational Method for Blunt Body Flows," AIAA Journal, Vol 4, No. 12, Dec. 1966, p 2136-2141
5. Moretti, G. and Bleich, G., "Three-Dimensional Flow Around Blunt Bodies," AIAA Journal, Vol 5, No. 9, Sep 1967, p 1557-1562
6. Van Dyke, Milton D., "The Supersonic Blunt Body Problem-- Review and Extension," Journal of the Aero/Space Sciences, Aug 1958, p 485-495
7. Van Dyke, Milton D., "The Blunt Body Problem Revisited," in Fundamental Phenomena in Hypersonic Flow, edited by J. Gordon Hall, Cornell University Press, New York, p 52-65
8. McNamara, William, "FLAME Computer Code for the Axisymmetric Interaction of a Blast Wave with a Shock Layer on a Blunt Body," Journal of Spacecraft and Rockets, Vol 4, No. 6, Jun. 1967, p 790-795
9. Billig, Frederick S., "Shock Wave Shapes Around Spherical and Cylindrical Nosed Bodies," Journal of Spacecraft and Rockets, Vol 4, No. 6, Jun. 1967, p 822-823
10. Lees, Lester, "Hypersonic Flow," in Fifth International Aeronautical Conference, Los Angeles - 1955, Institute of the Aeronautical Sciences, New York, 1955, p 241-276
11. Fuller, F. B., "Numerical Solutions for Supersonic Flow of an Ideal Gas Around Blunt Two-Dimensional Bodies," NASA TN-D-791, 1961
12. Li, T. Y., and Geiger, R. E., "Stagnation Point of a Blunt Body in Hypersonic Flow," Journal of Aeronautical Sciences, Vol 24, Jan. 1957, p 25-32
13. Abbett, M., private communication, Dec. 1967
14. Van Dyke, M., Perturbation Methods in Fluid Mechanics, Academic Press, New York, 1964, p 202
15. Lomax, H and Inouye, M., "Numerical Analysis of Flow Properties About Blunt Bodies Moving at Supersonic Speeds in an Equilibrium Gas," NASA TR-R-204, Jul 1964
16. Roberts, J. F., Lewis, C. H. and Reed, M., "Ideal Gas Spherically Blunted Cone Flow Field Solutions at Hypersonic Conditions," AEDC-TR-66-121, Aug 1966
17. Van Tuyl, A. H., "Use of Rational Approximations in the Calculations of Flows Past Blunt Bodies," AIAA Journal, Vol 5, No. 2, Feb. 1967, p 218-225; also private communication

NOLTR 68-129

18. Stallings, R. L., Jr., "Experimentally Determined Local Flow Properties and Drag Coefficients for a Family of Blunt Bodies at Mach Numbers from 2.49 to 4.63," NASA TR-R-274, Oct 1967
19. Moretti, Gino, "Inviscid Blunt Body Shock Layers," PIBAL Report No. 68-15, Jun 1968, Polytechnic Institute of Brooklyn



1a.



1b.

FIG. 1 COORDINATE SYSTEM

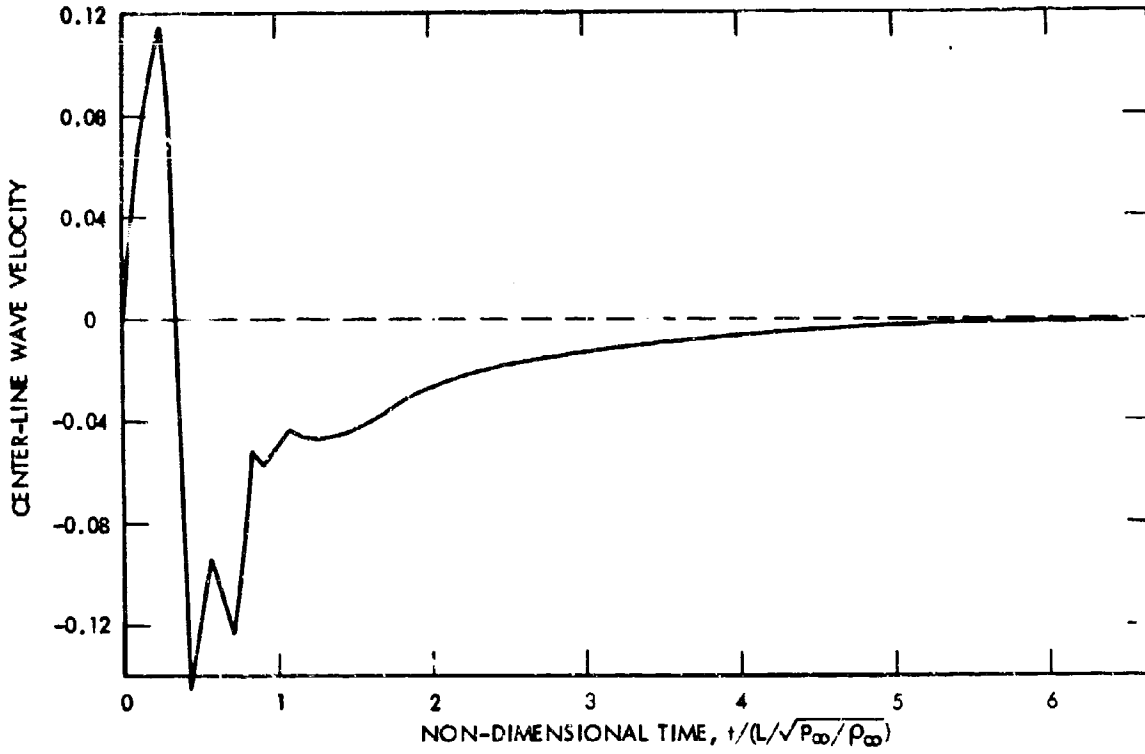


FIG. 2 TIME VARIATION OF WAVE VELOCITY; PARABOLIC CYLINDER, $M_\infty = 4$

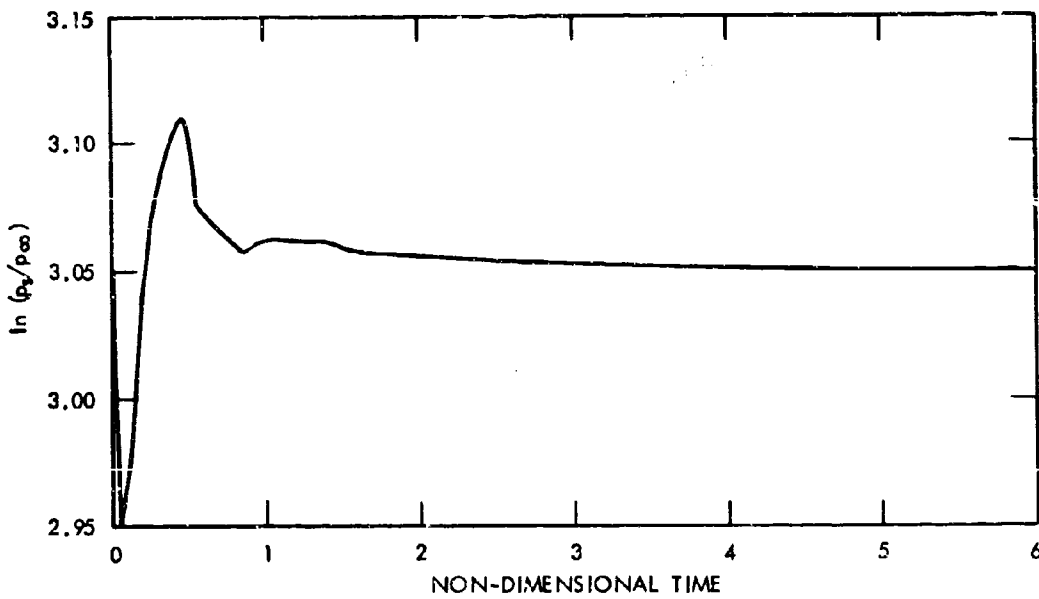


FIG. 3 TIME VARIATION OF STAGNATION POINT PRESSURE; PARABOLIC CYLINDER, $M_\infty = 4$

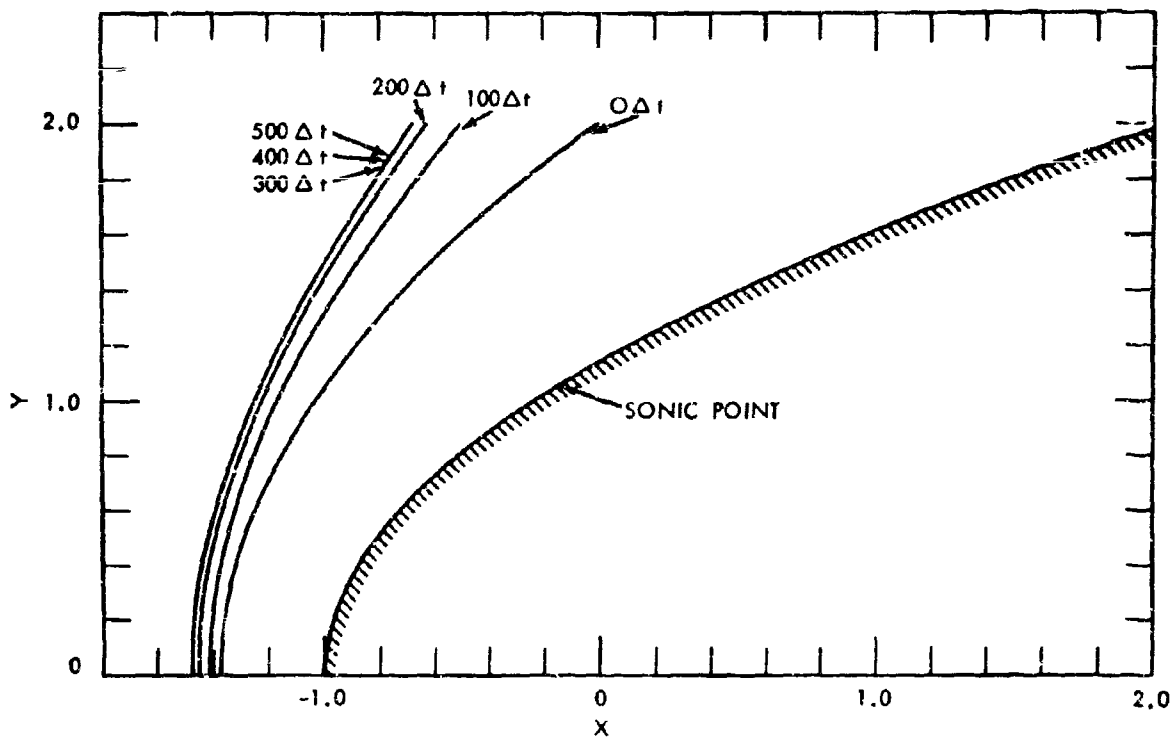


FIG. 4 TIME DEPENDENT SHOCK WAVE MOTION, PARABOLIC CYLINDER, $M_\infty = 4$

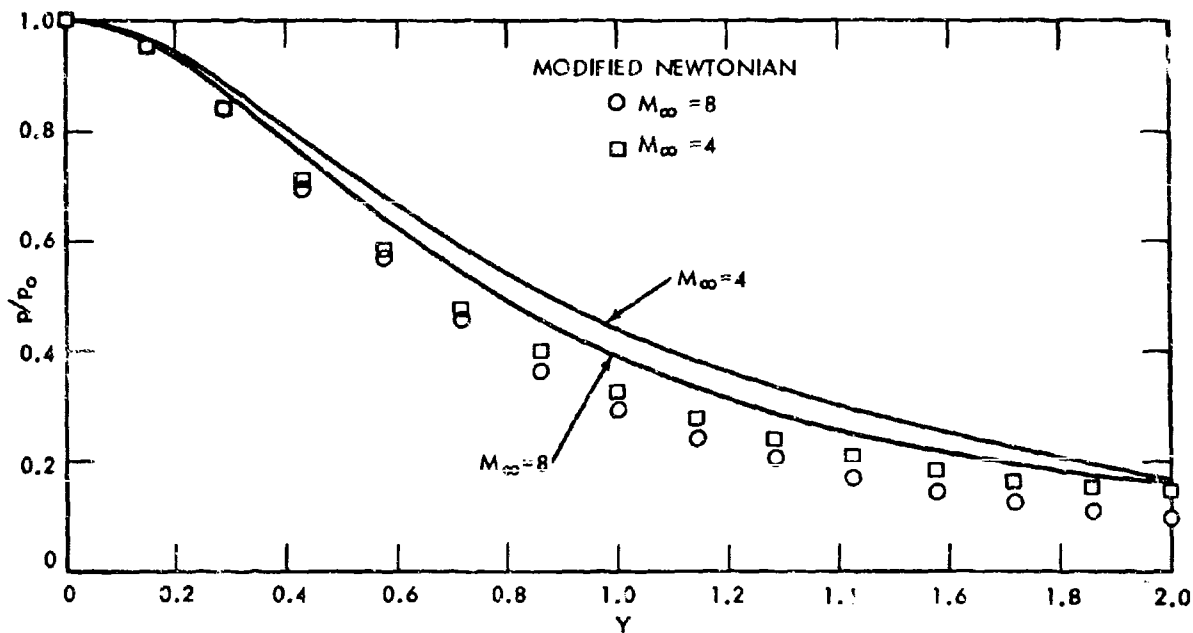


FIG. 5 SURFACE PRESSURE DISTRIBUTIONS, PARABOLIC CYLINDER

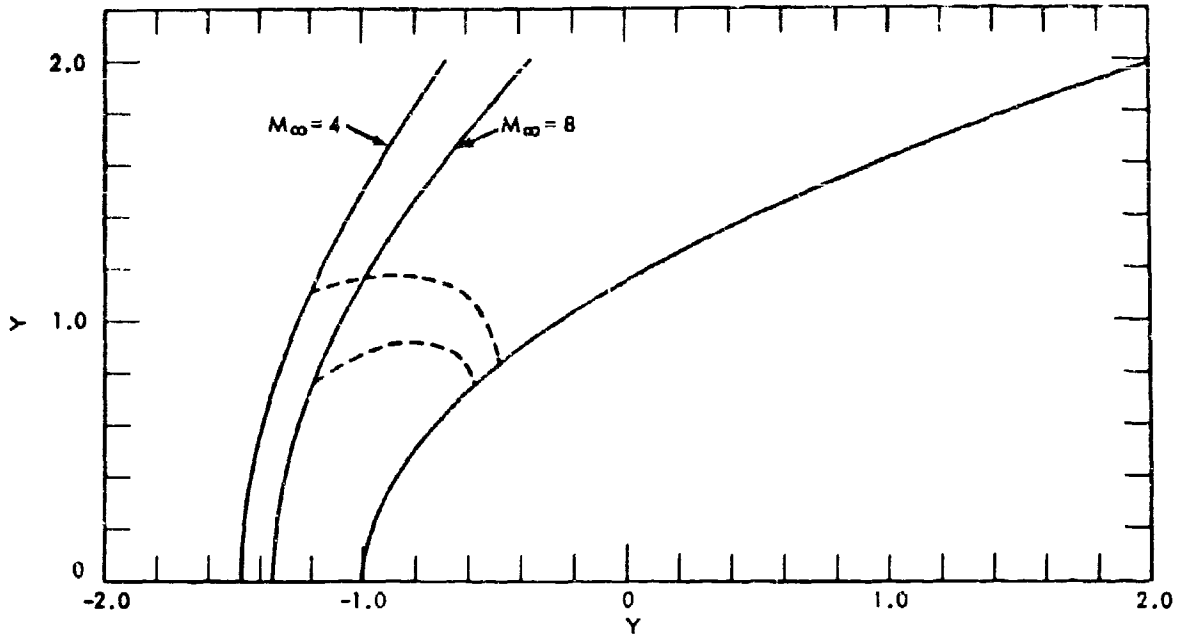


FIG. 6 SHOCK SHAPES AND SONIC LINES; PARABOLIC CYLINDER

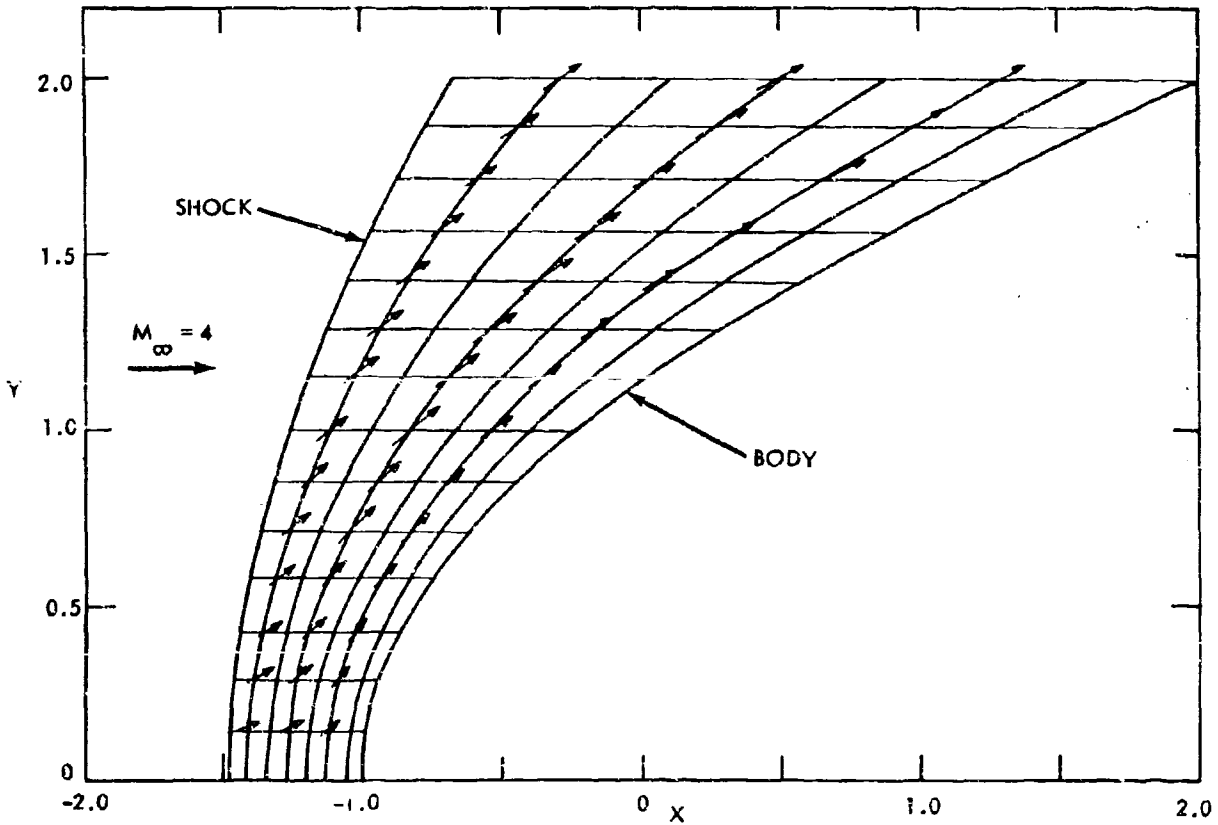


FIG. 7 VELOCITY DIRECTION FIELD; PARABOLIC CYLINDER

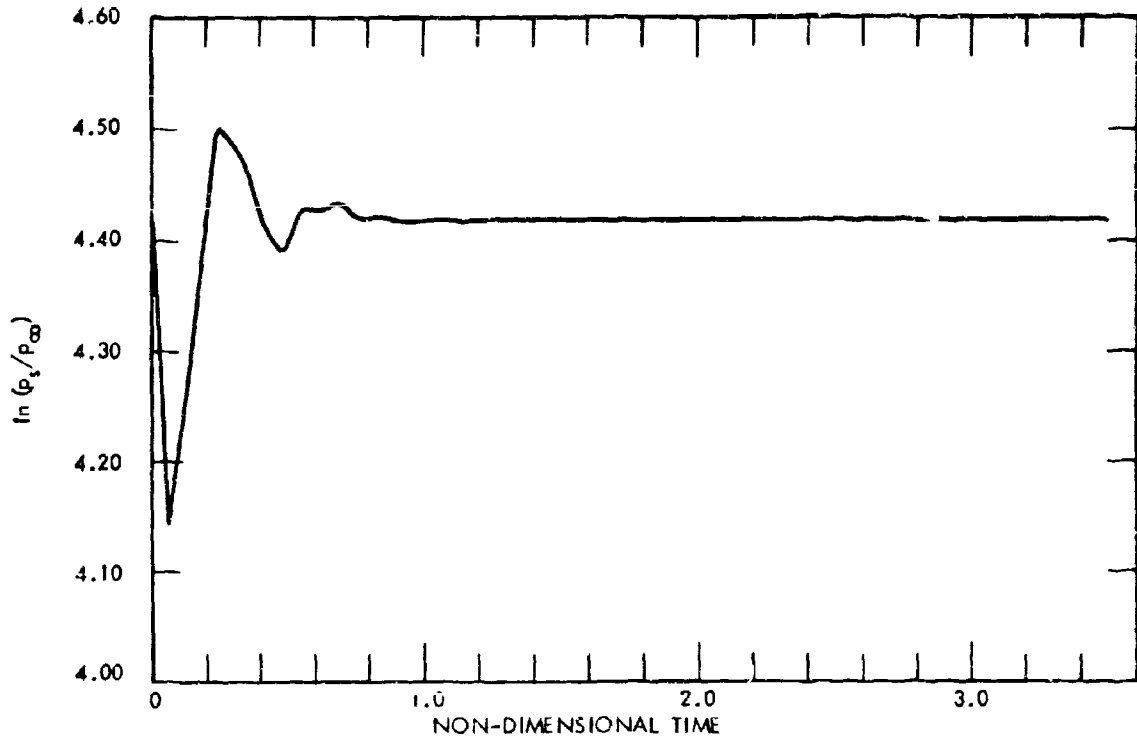


FIG. 8 TIME VARIATION OF STAGNATION POINT PRESSURE, PARABOLIC CYLINDER, $M_\infty = 8$

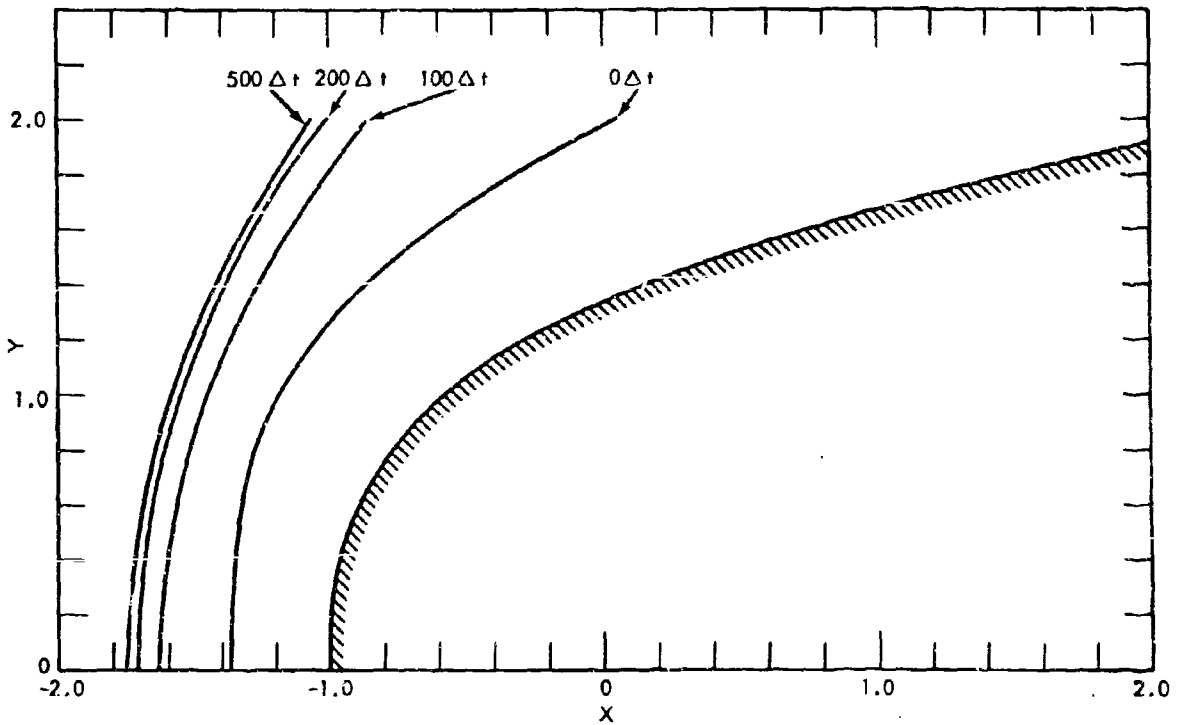


FIG. 9 TIME DEPENDENT SHOCK WAVE MOTION; CUBIC CYLINDER, $M_\infty = 4$

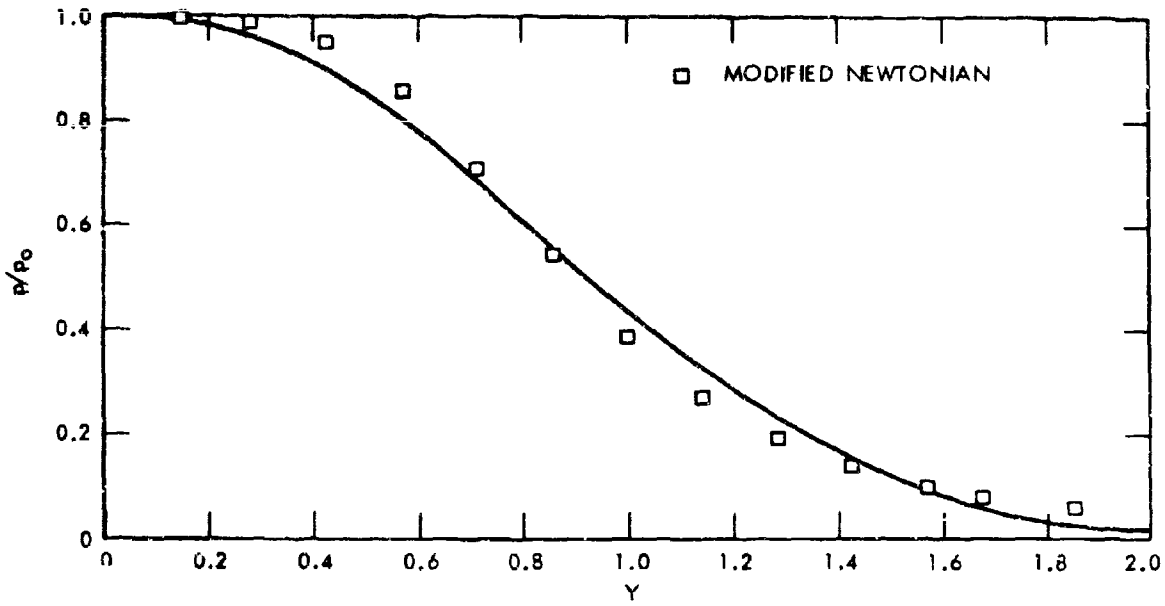


FIG. 10 SURFACE PRESSURE DISTRIBUTION; CUBIC BODY, $M_\infty = 4$

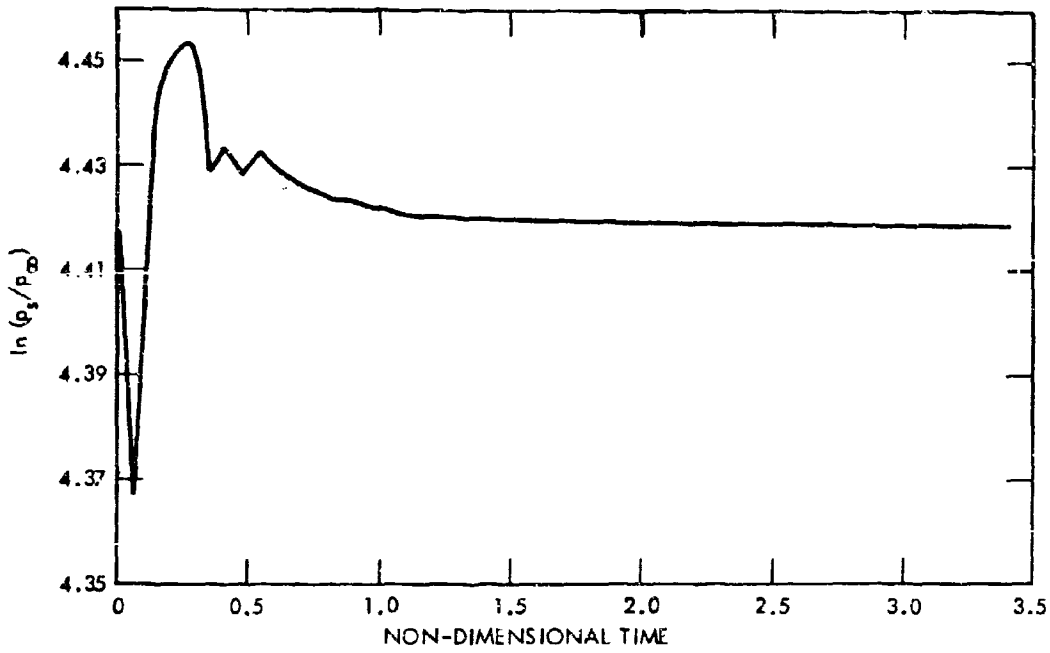


FIG. 11 TIME VARIATION OF STAGNATION POINT PRESSURE; BLUNTED WEDGE, $M_\infty = 8$

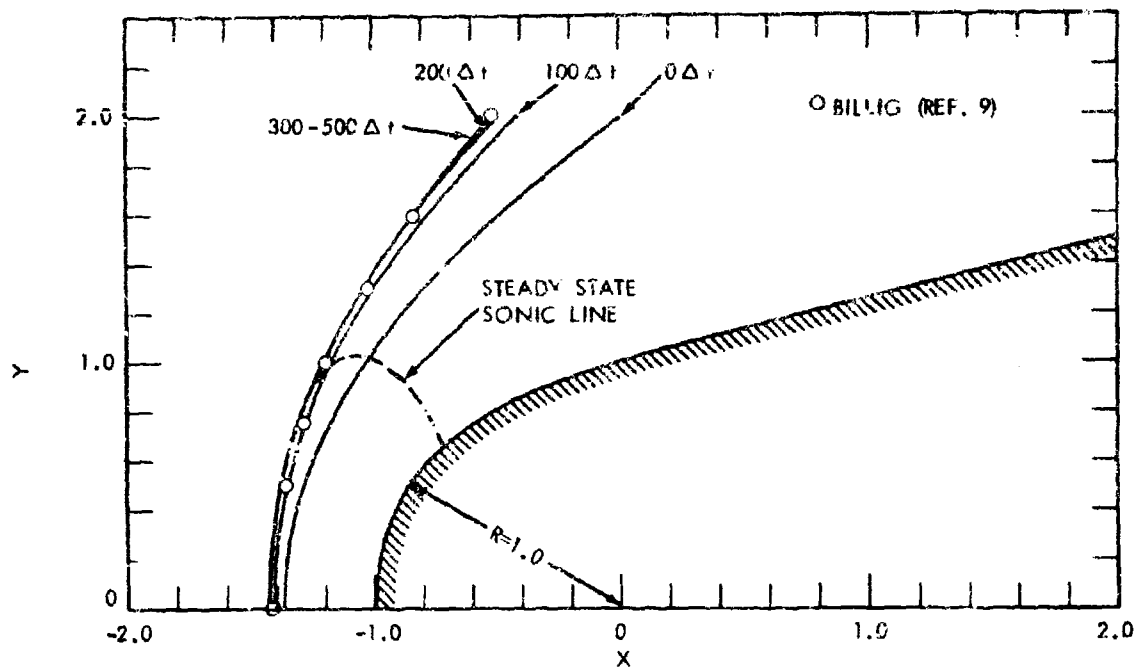


FIG. 12 TIME DEPENDENT SHOCK WAVE MOTION; BLUNTED WEDGE, $M_\infty = 8$

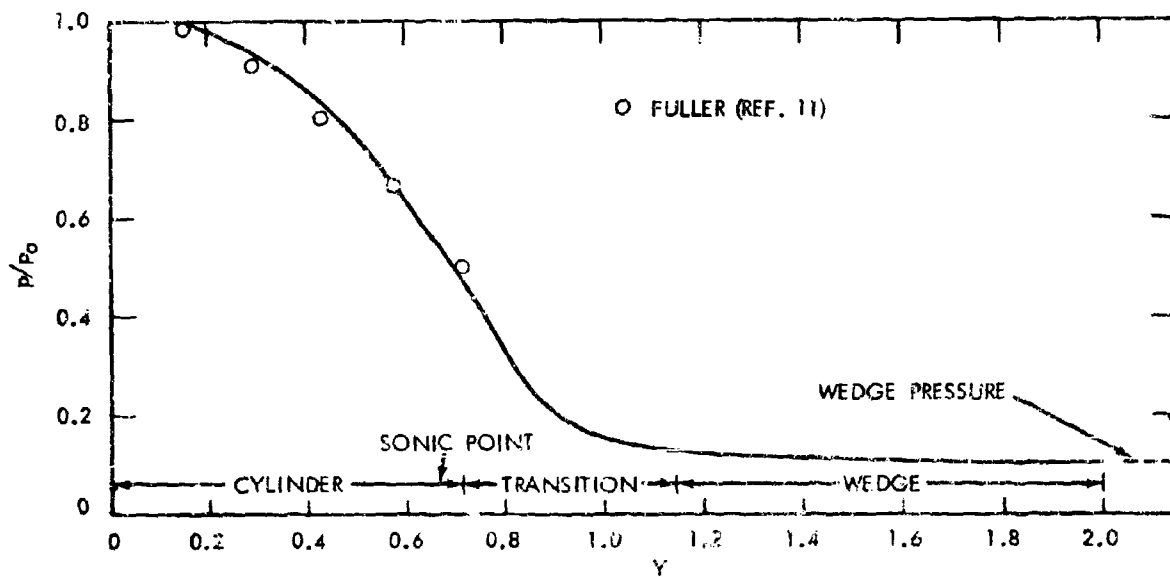


FIG. 13 SURFACE PRESSURE DISTRIBUTION; BLUNTED WEDGE, $M_\infty = 8.0$

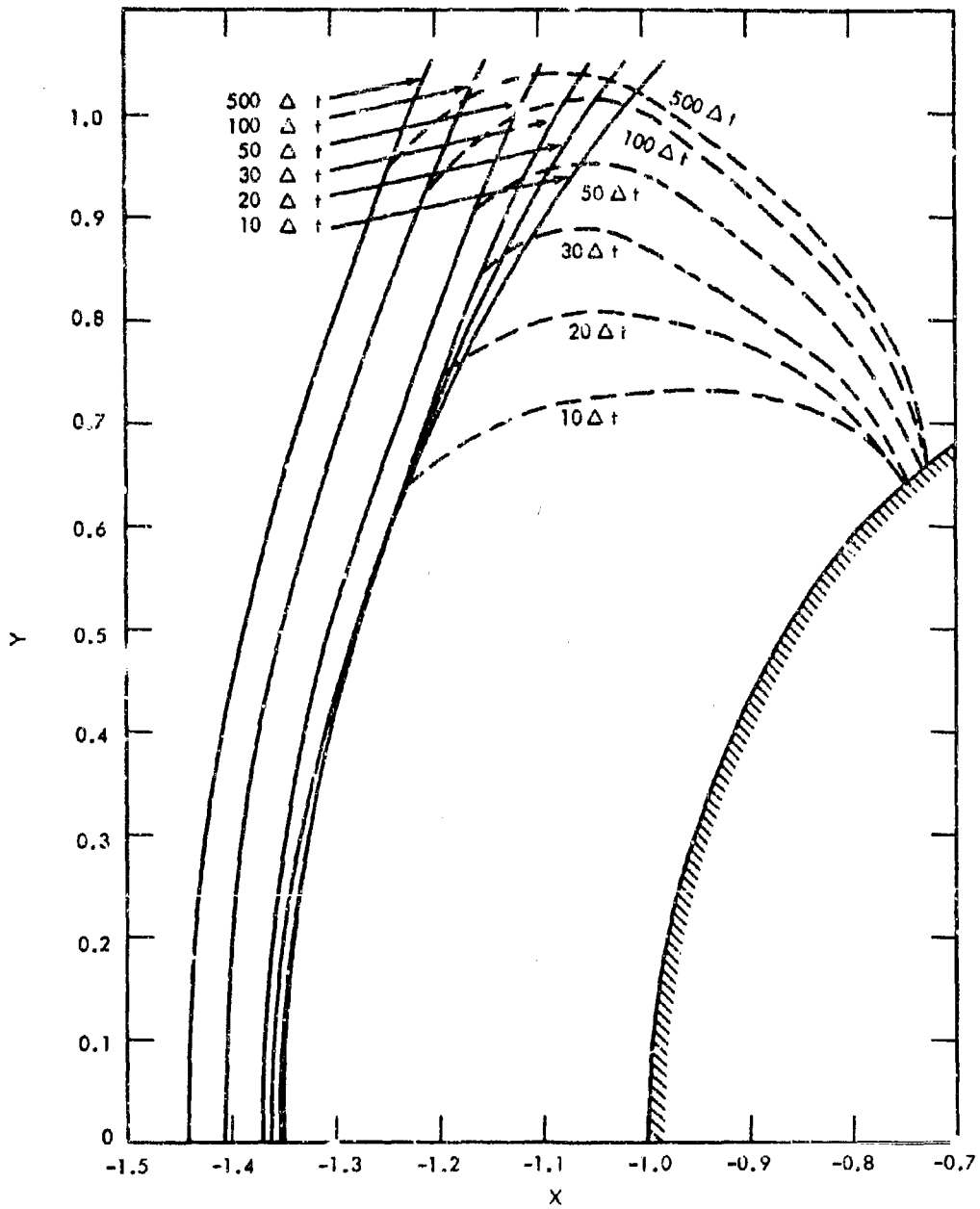


FIG. 14 SONIC LINE TIME VARIATION; BLUNTED WEDGE, $M_\infty = 8$

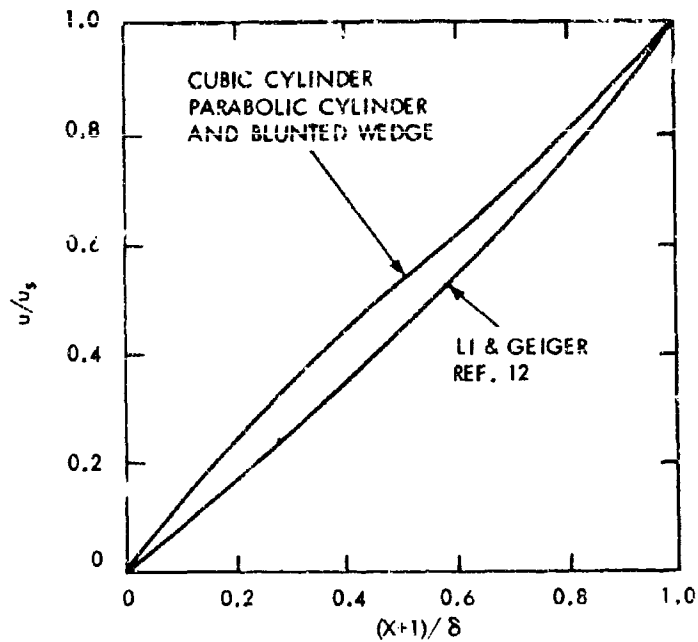


FIG. 15 VELOCITY VARIATION ALONG THE STAGNATION STREAMLINE

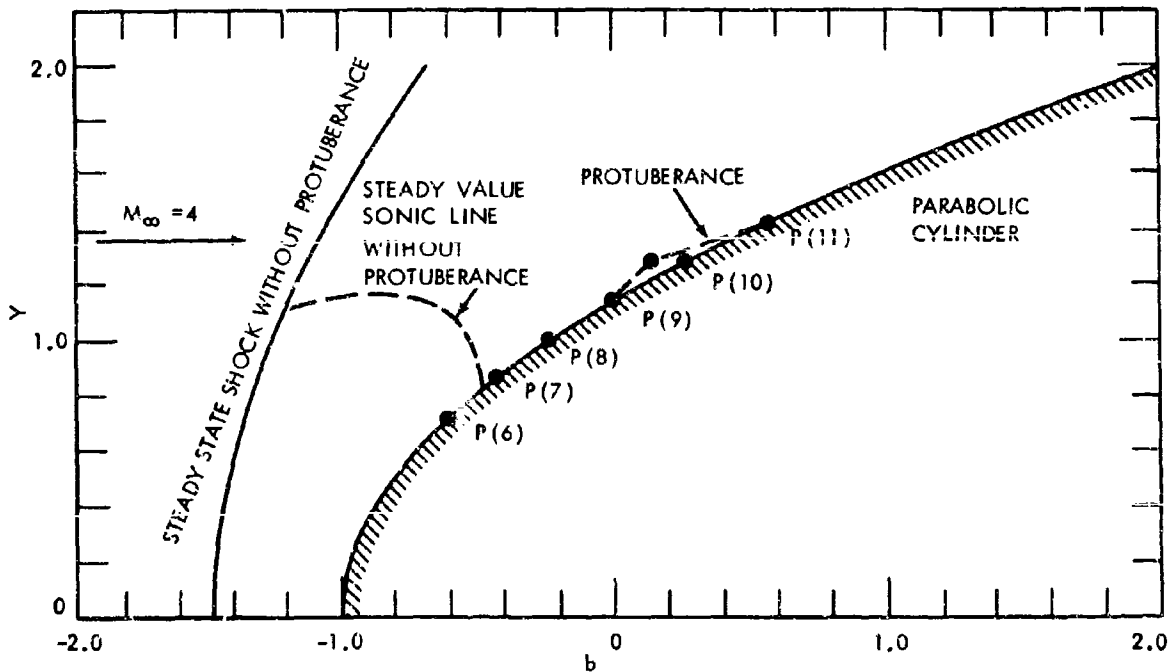


FIG. 16 CONFIGURATION FOR PROTUBERANCE EXPERIMENT

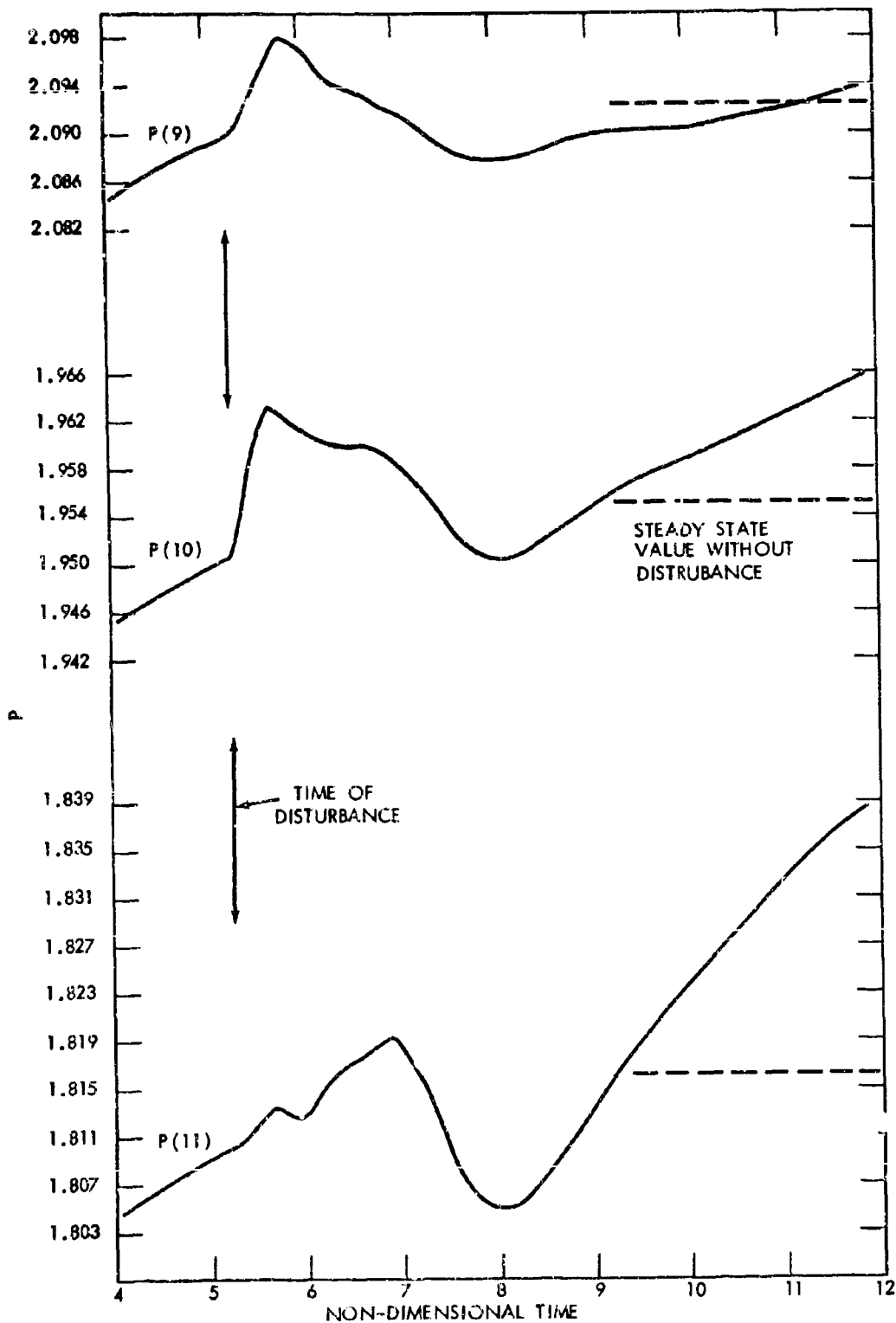


FIG. 17 DISTURBED SURFACE PRESSURE VARIATIONS

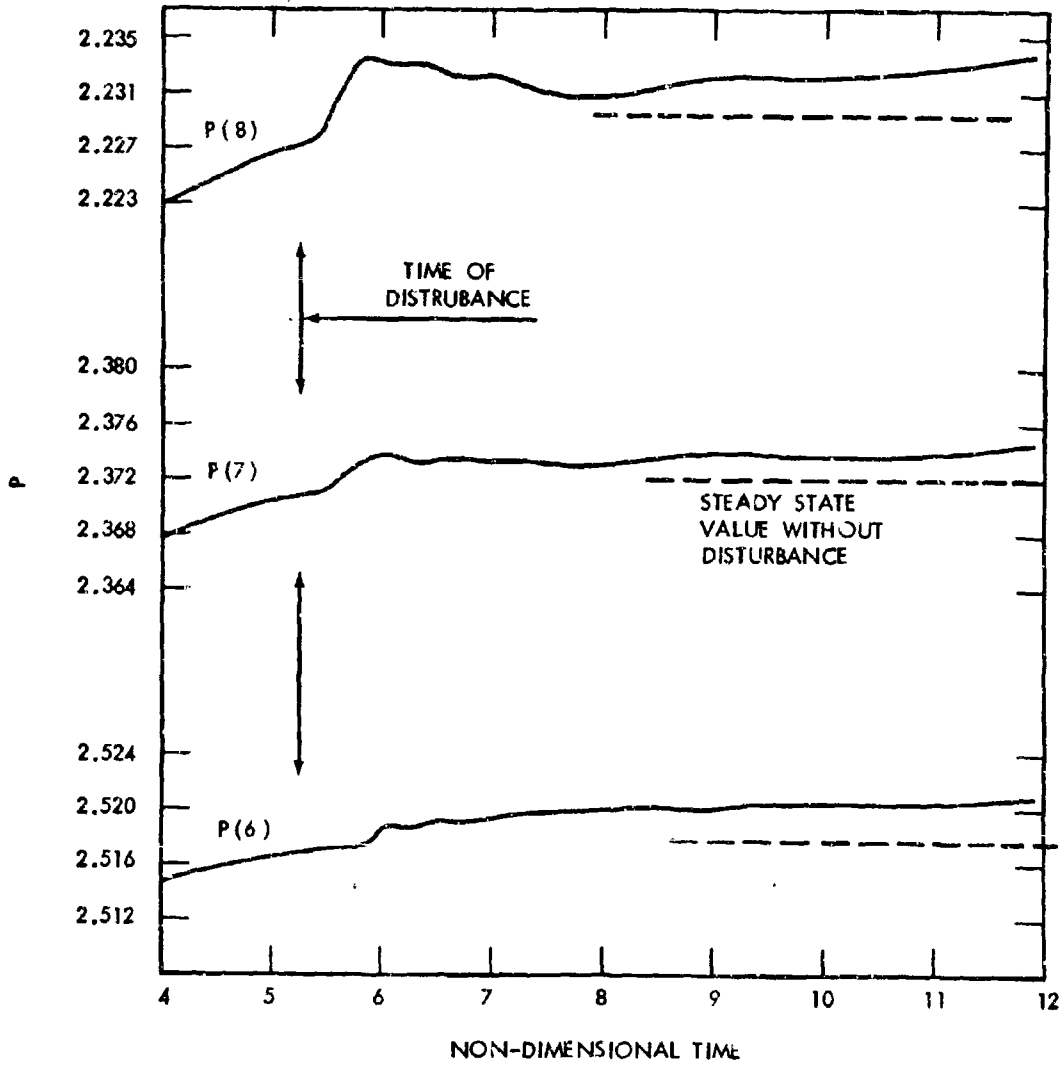


FIG. 18 DISTURBED SURFACE PRESSURE VARIATIONS , CONT.

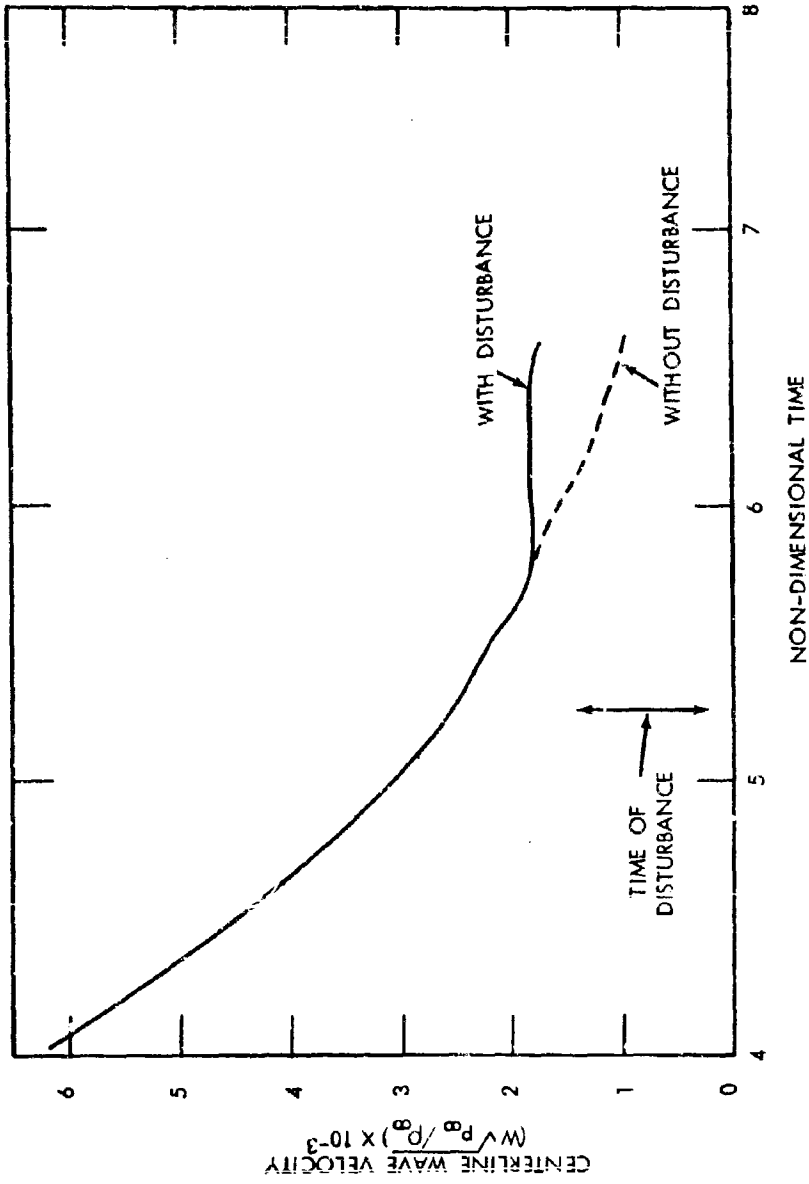


FIG. 19 CENTERLINE WAVE VELOCITY WITH AND WITHOUT DISTURBANCE

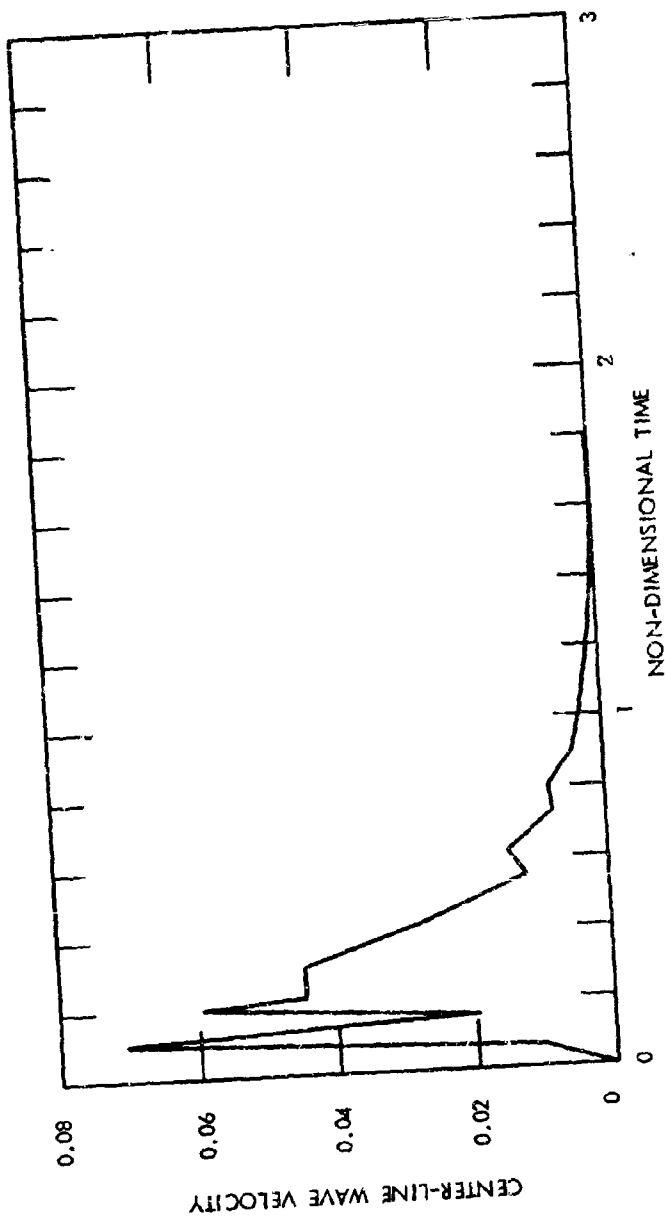


FIG. 20 TIME VARIATION OF WAVE VELOCITY; PARABOLOID, $M_{\infty} = 4$

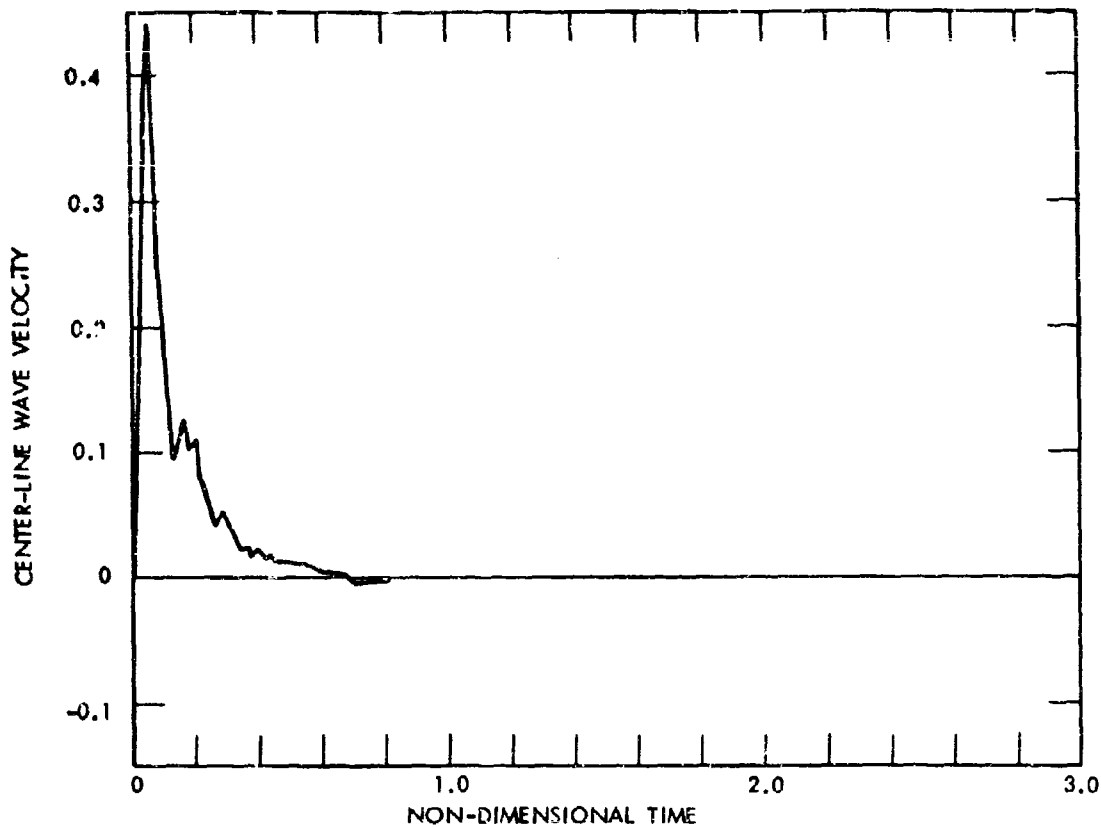


FIG. 21 TIME VARIATION OF WAVE VELOCITY; PARABOLOID, $M_\infty = 8$

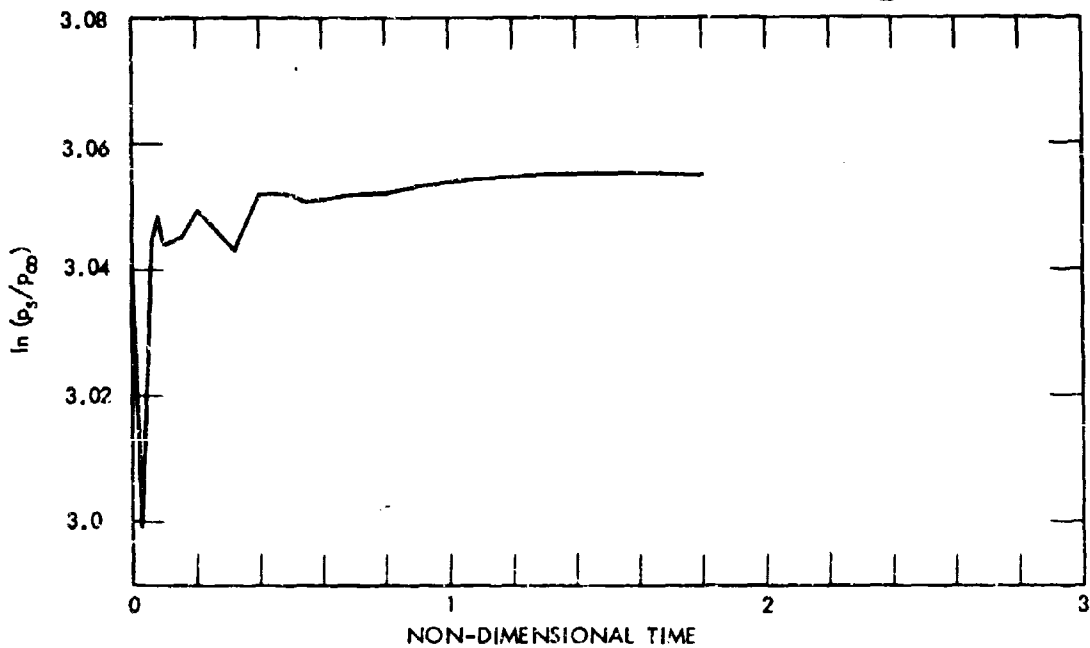


FIG. 22 TIME VARIATION OF STAGNATION POINT PRESSURE; PARABOLOID, $M_\infty = 4$

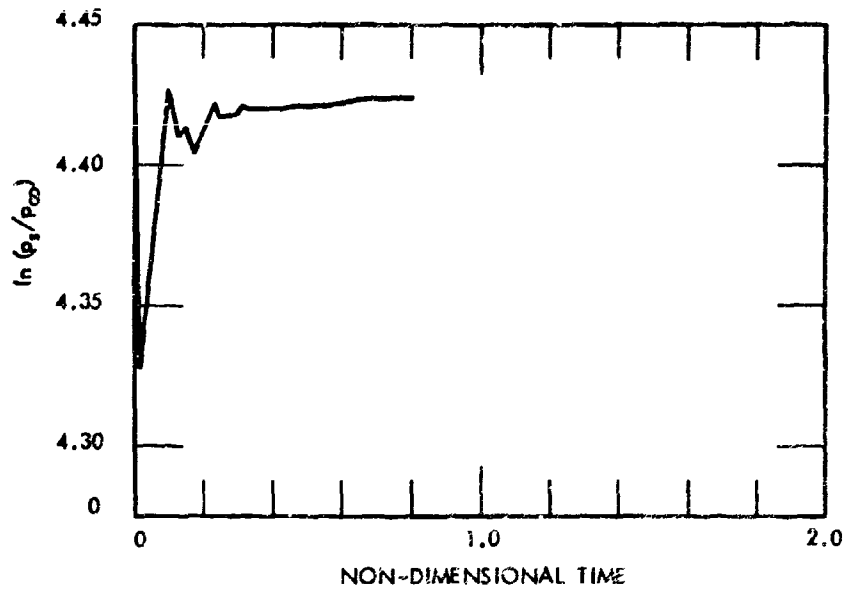


FIG. 23 TIME VARIATION OF STAGNATION POINT PRESSURE, PARABOLOID, $M_\infty = 8$

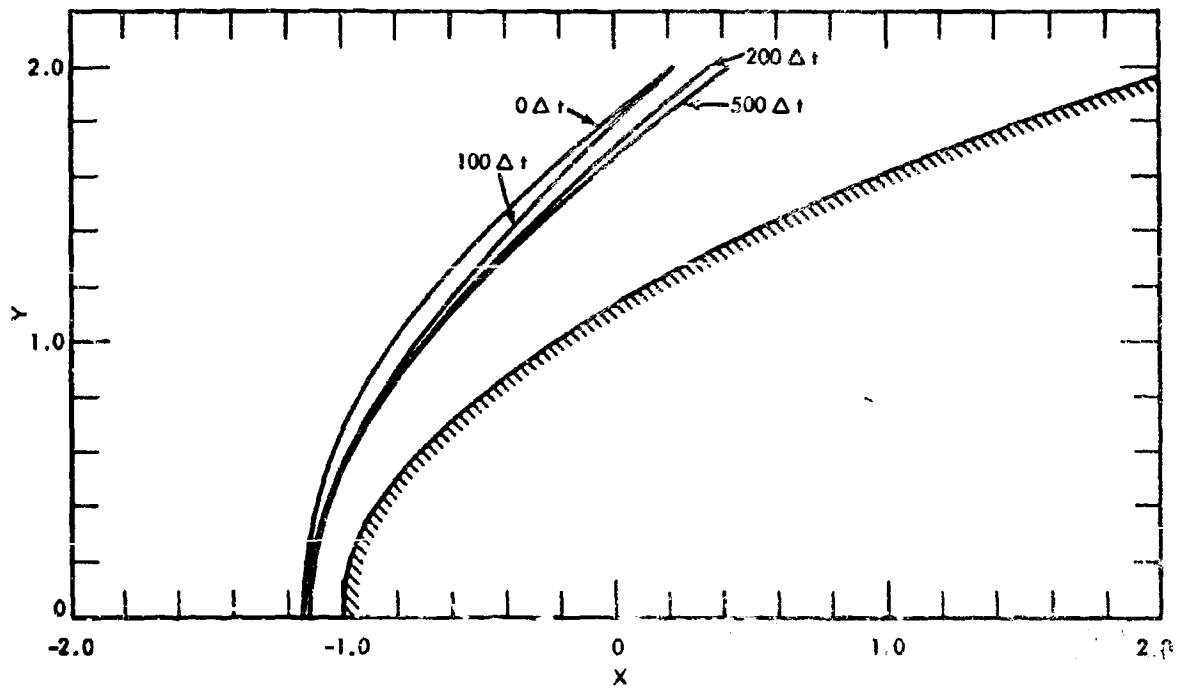


FIG. 24 TIME DEPENDENT SHOCK WAVE MOTION, PARABOLOID, $M_\infty = 4$

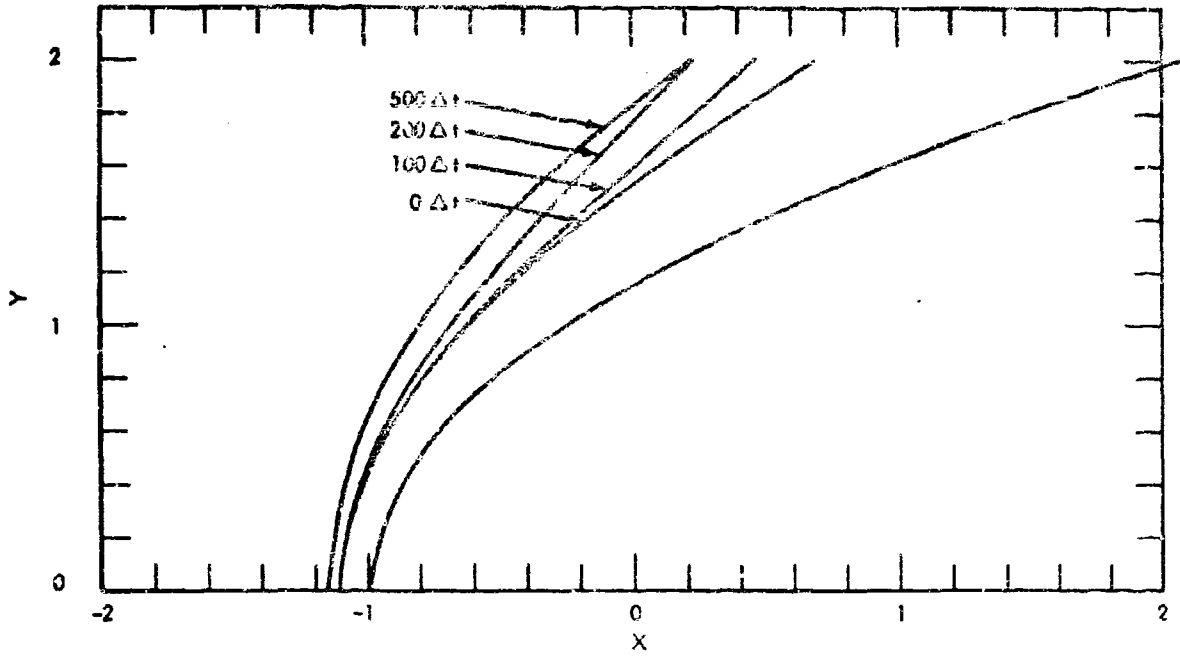


FIG. 25 TIME DEPENDENT SHOCK WAVE MOTION; PARABOLOID, $M_\infty = 8$

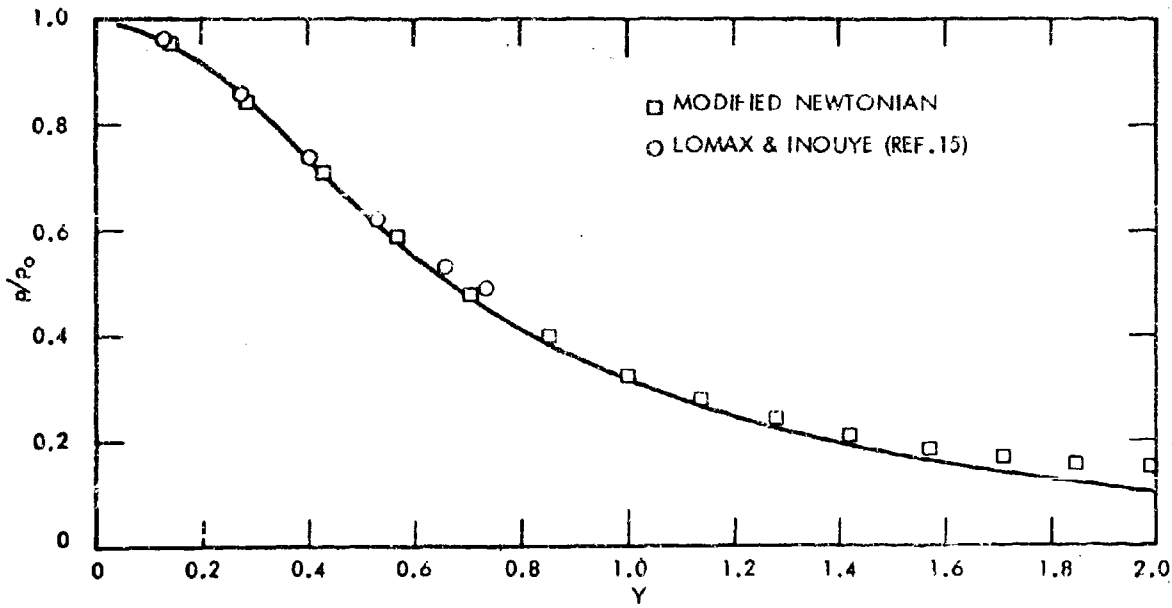


FIG. 26 SURFACE PRESSURE DISTRIBUTION; PARABOLOID, $M_\infty = 4$

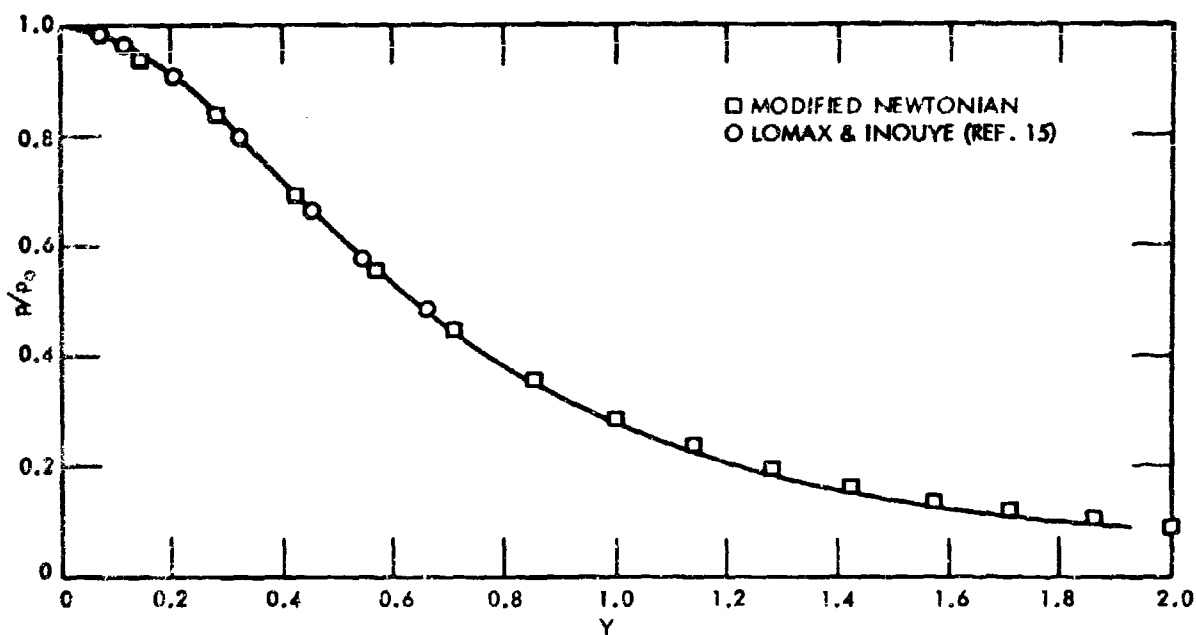


FIG. 27 SURFACE PRESSURE DISTRIBUTION, PARABOLOID, $M_\infty = 8$

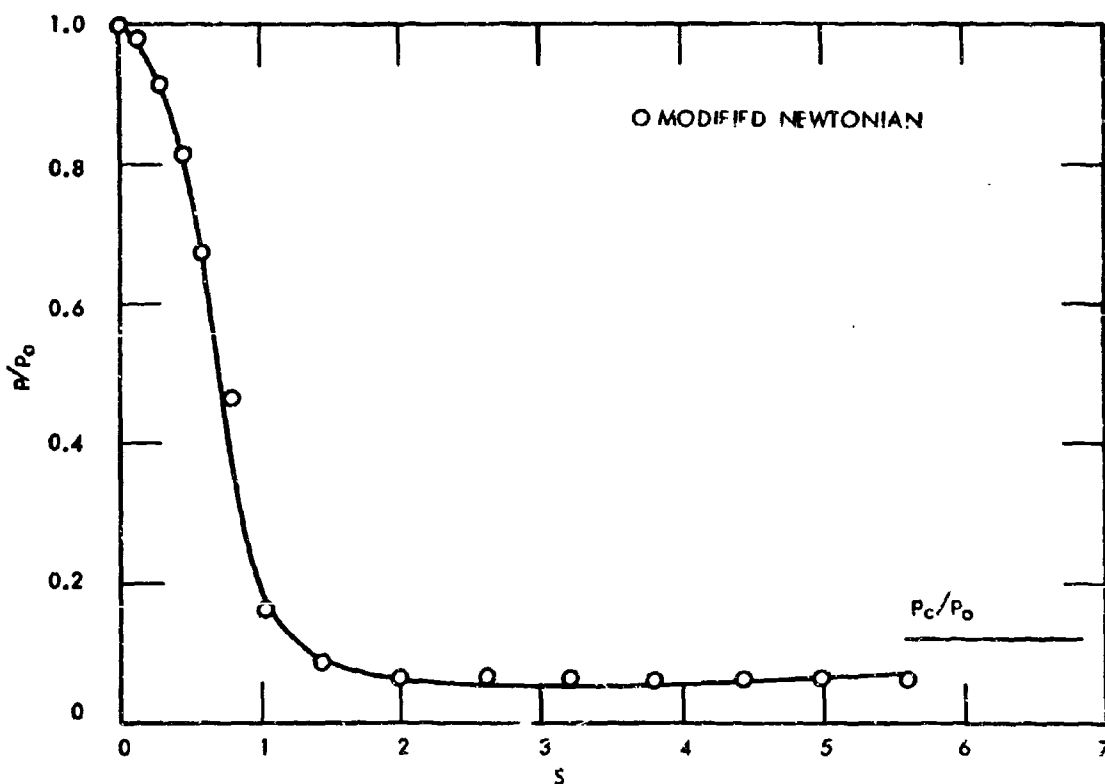


FIG. 28 SURFACE PRESSURE DISTRIBUTION, SPHERE-CONE, $M_\infty = 4$

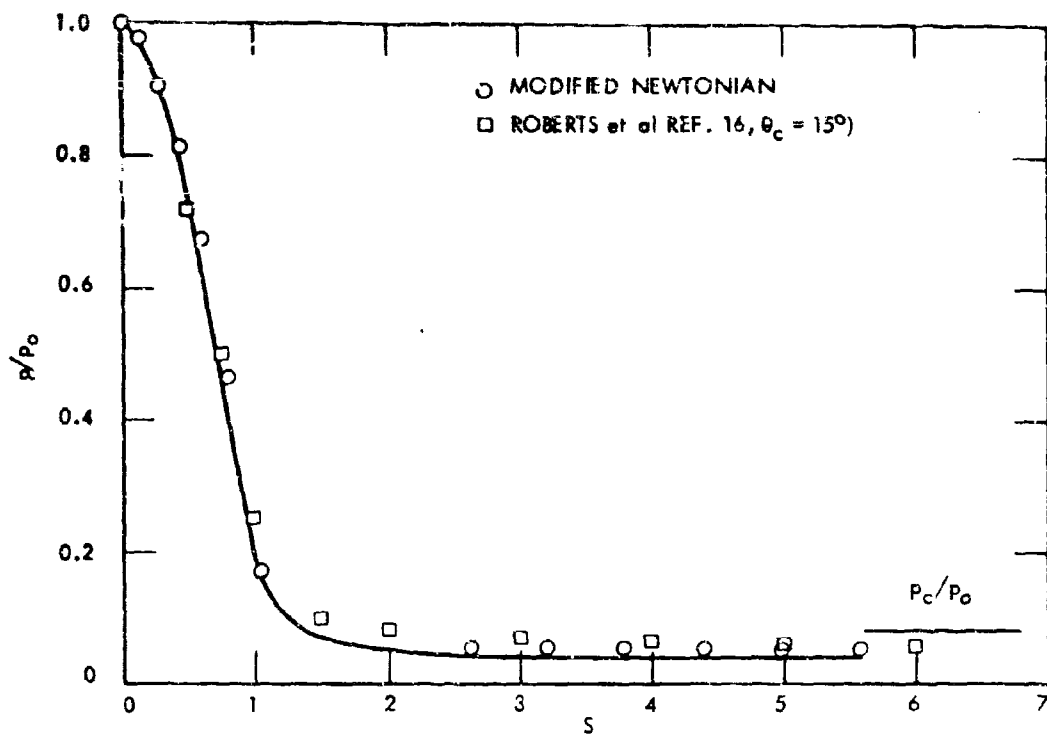


FIG. 29 SURFACE PRESSURE DISTRIBUTION; SPHERE-CONE, $M_\infty = 8$

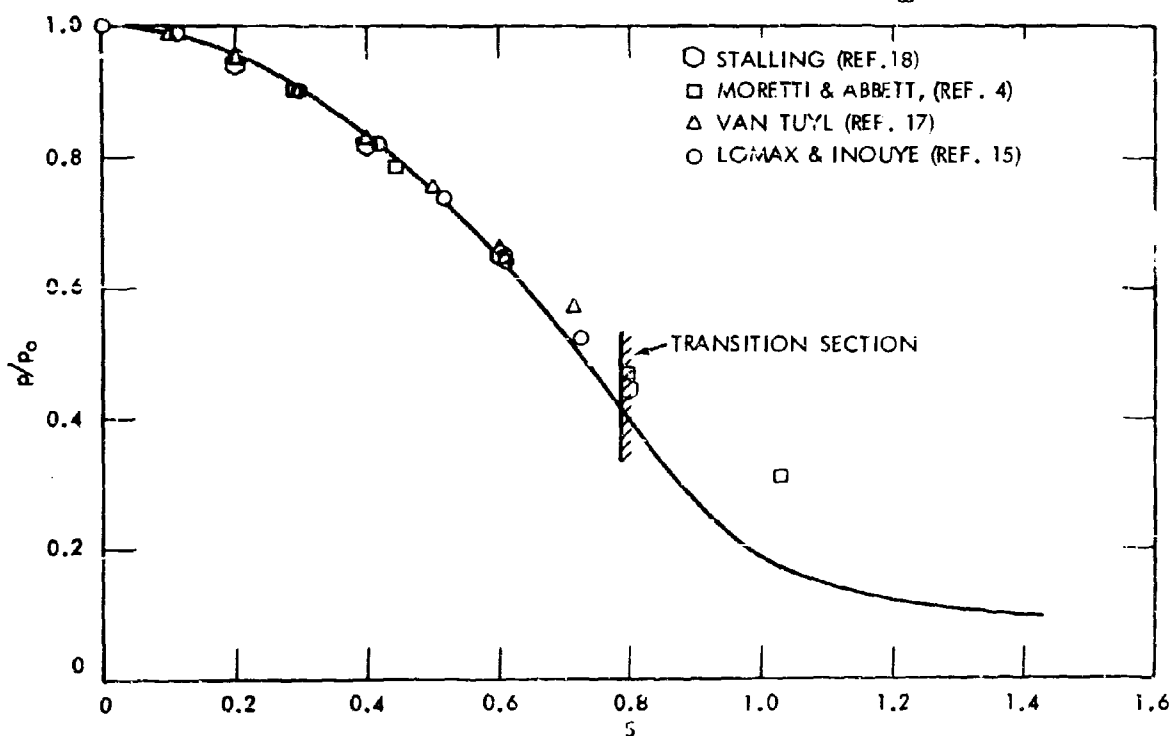


FIG. 30 SURFACE PRESSURE DISTRIBUTION (EXPANDED SCALE); SPHERE-CONE, $M_\infty = 4$

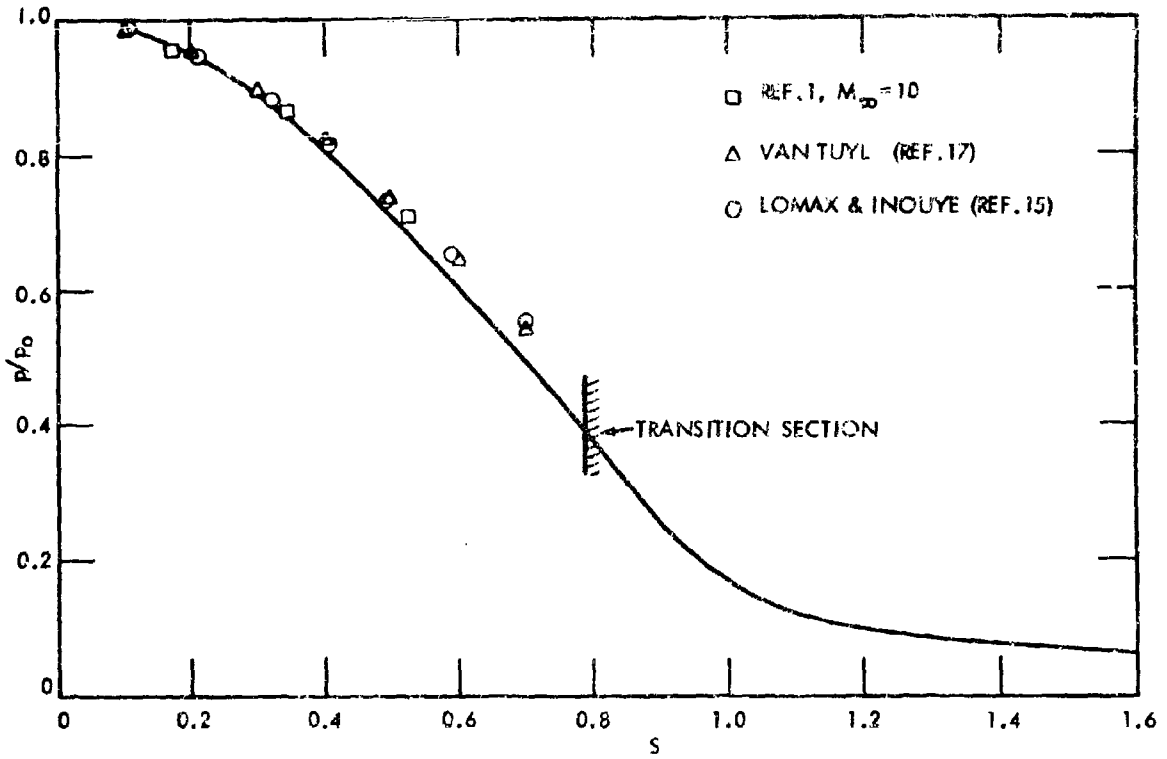


FIG. 31 SURFACE PRESSURE DISTRIBUTION (EXPANDED SCALE), SPHERE-CONE, $M_\infty = 8$

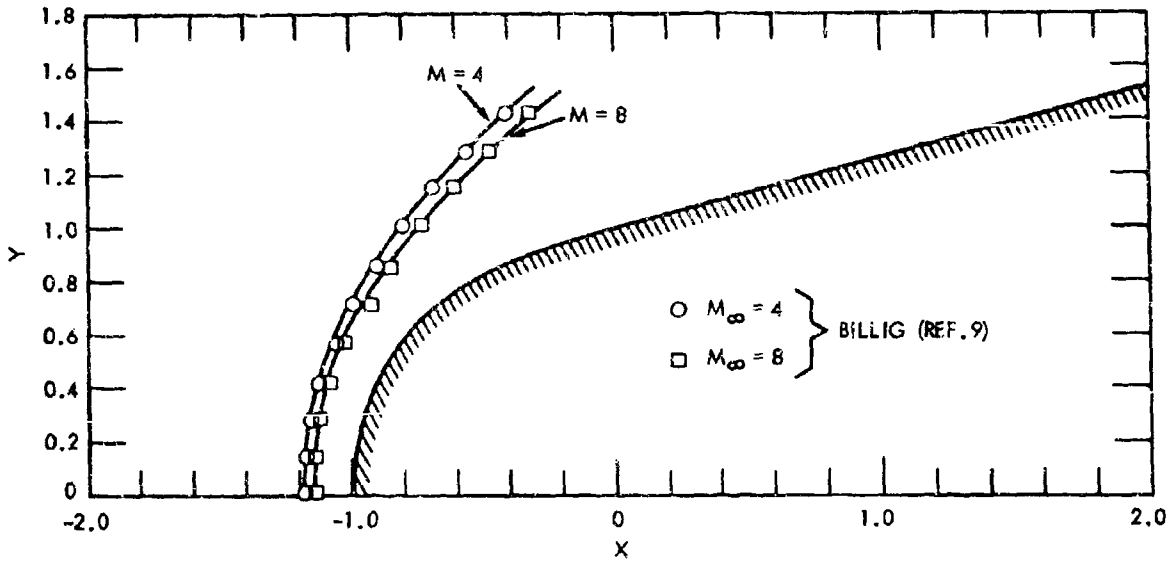


FIG. 32 SHOCK WAVE SHAPES; SPHERE-CONE

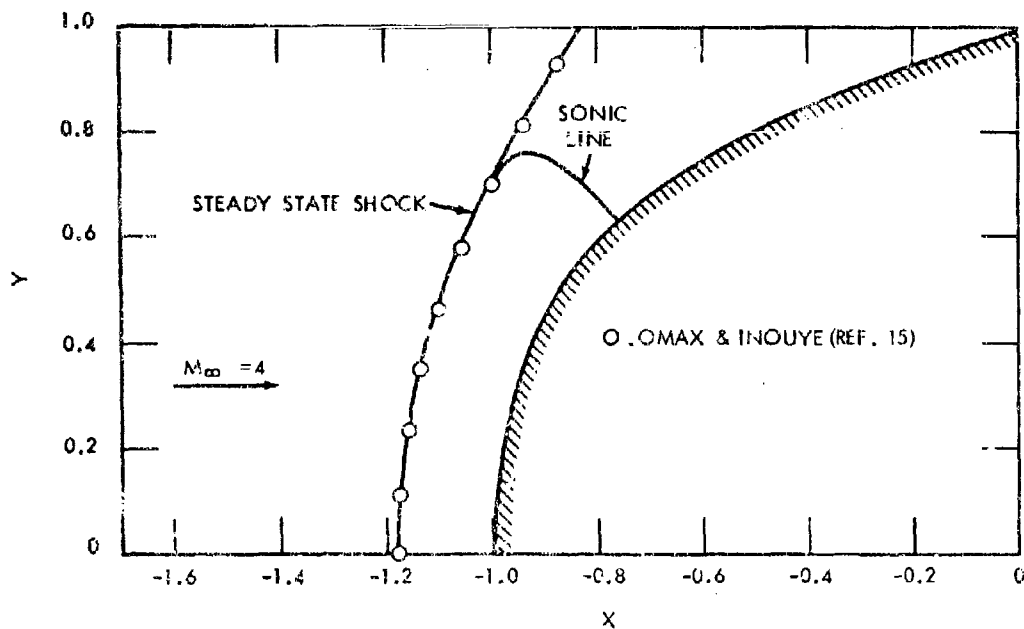


FIG. 33 SHOCK WAVE SHAPE AND SONIC LINE; SPHERE-CONE, $M_\infty = 4$

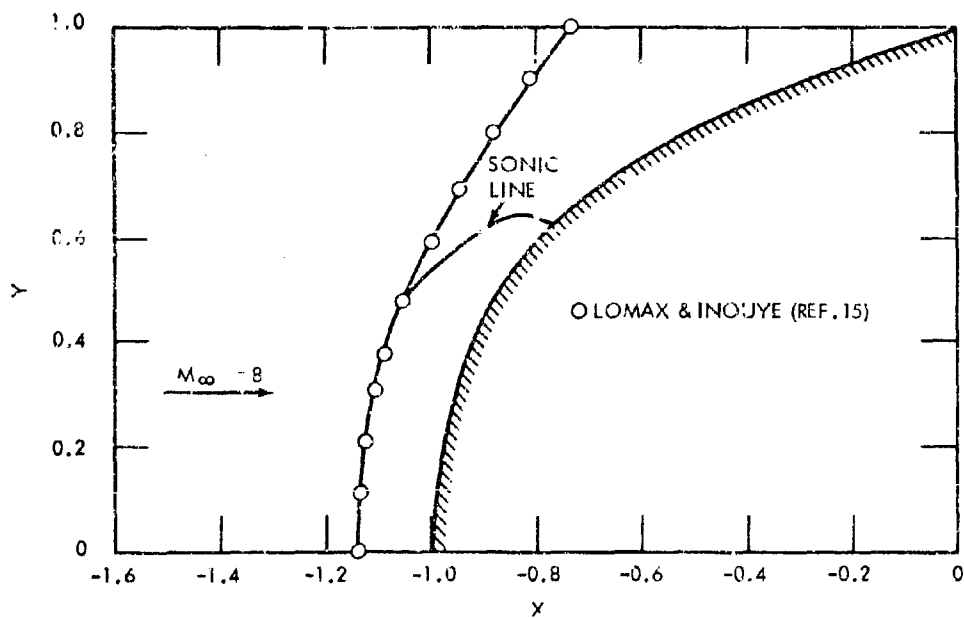


FIG. 34 SHOCK WAVE AND SONIC LINE; SPHERE-CONE, $M_\infty = 8$

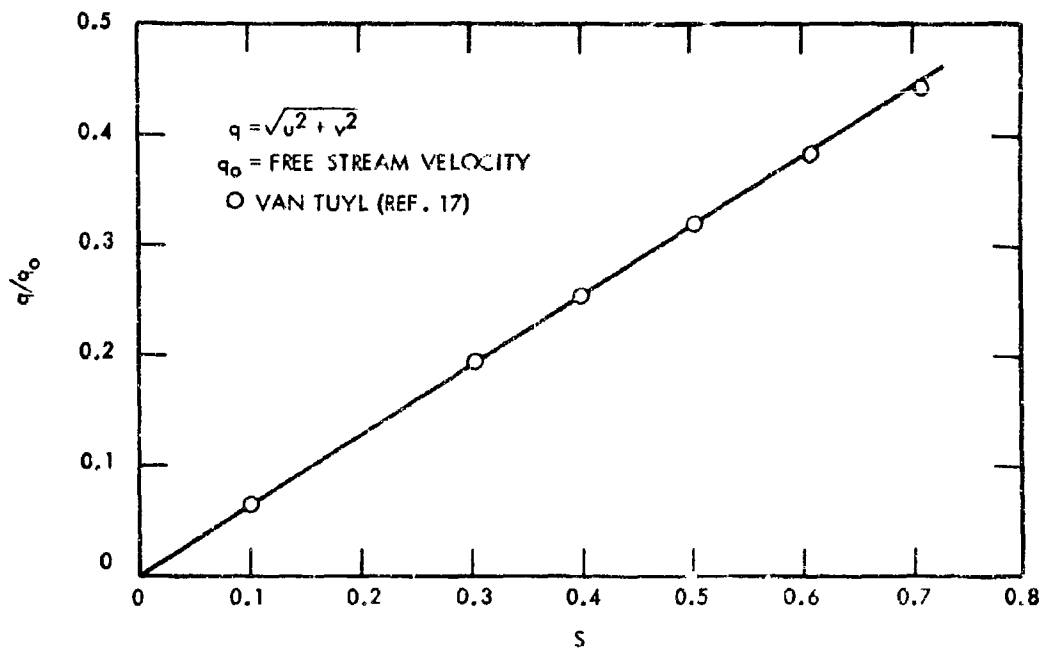


FIG. 35 VELOCITY DISTRIBUTION; SPHERE-CONE; $M_\infty = 4$

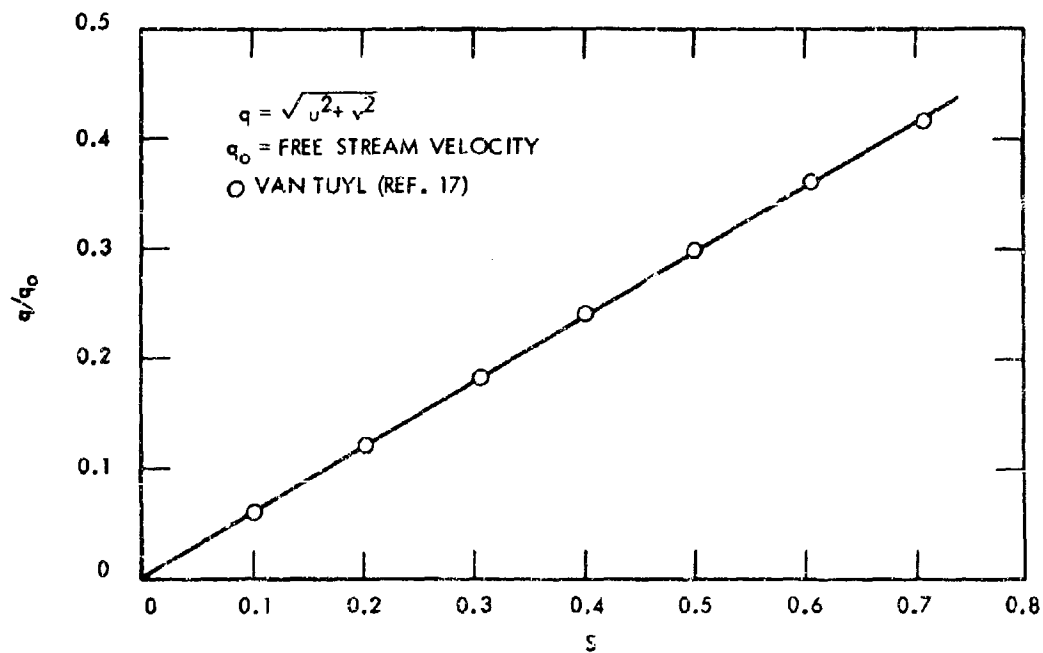


FIG. 36 VELOCITY DISTRIBUTION; SPHERE-CONE, $M_\infty = 8$

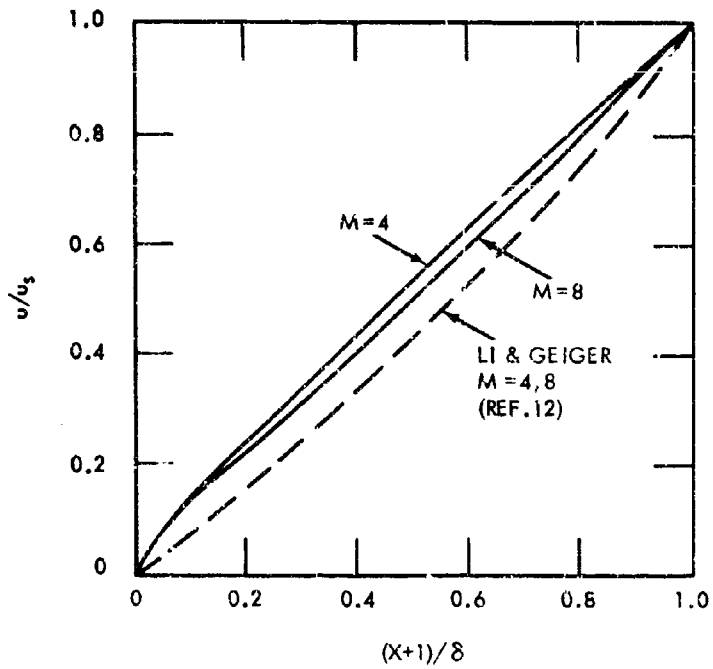


FIG. 37 VELOCITY VARIATION ALONG STAGNATION STREAMLINE; PARABOLOID

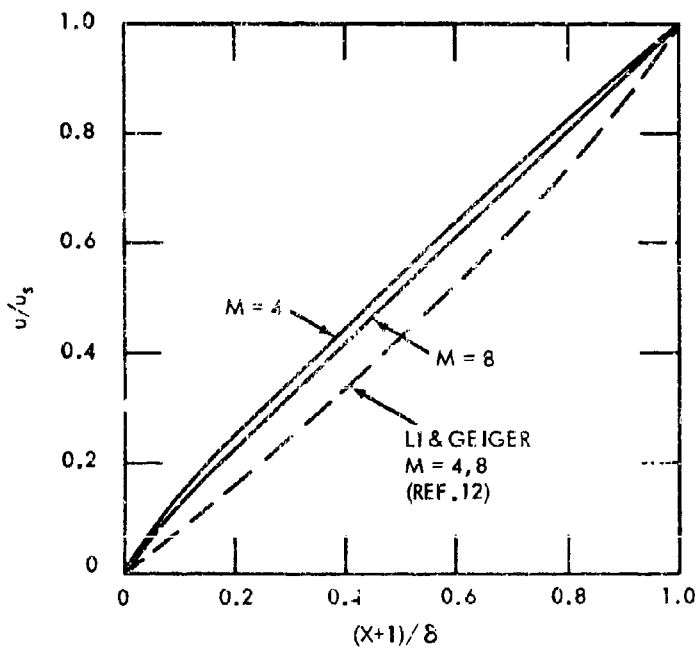


FIG. 38 VELOCITY VARIATION ALONG STAGNATION STREAMLINE; SPHERE-CONE

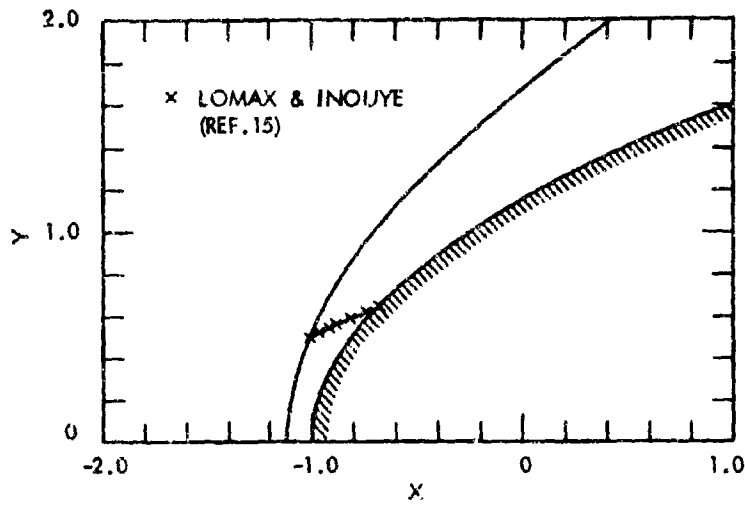


FIG. 39 SONIC LINE; PARABOLOID, $M_\infty = 4$

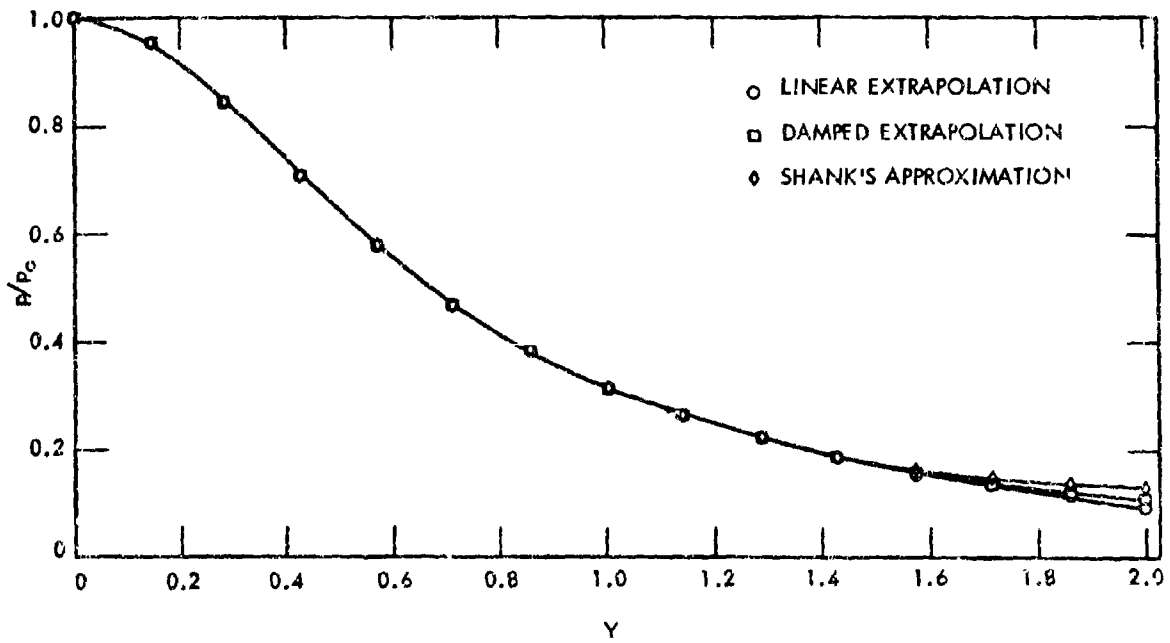


FIG. 40 EFFECT OF EXTRAPOLATION TO UPPER BOUNDARY ON PRESSURE DISTRIBUTION; PARABOLOID, $M_\infty = 4$

UNCLASSIFIED

Security Classification

DOCUMENT CONTROL DATA - R & D		
<i>(Security classification of title, body of abstract and indexing annotation must be entered when the overall report is classified)</i>		
1. ORIGINATING ACTIVITY (Corporate author)	20. REPORT SECURITY CLASSIFICATION	
U. S. Naval Ordnance Laboratory White Oak, Silver Spring, Maryland	UNCLASSIFIED	
	20. GROUP	
1. REPORT TITLE		
ON HYPERSONIC BLUNT-BODY FLOW FIELDS OBTAINED WITH A TIME-DEPENDENT TECHNIQUE		
4. DESCRIPTIVE NOTES (Type of report and inclusive dates)		
final		
5. AUTHOR(S) (First name, middle initial, last name)		
J. D. Anderson, Jr., L. M. Albacete and A. E. Winkelmann		
6. REPORT DATE	76. TOTAL NO. OF PAGES	75. NO. OF REFS
22 October 1968	24 plus illus.	19
99. CONTRACT OR GRANT NO.	98. ORIGINATOR'S REPORT NUMBER(S)	
	NOLTR 68-129	
b. PROJECT NO.		
c.	99. OTHER REPORT NO(S) (Any other numbers that may be assigned this report)	
d.		
10. DISTRIBUTION STATEMENT		
This document is subject to special export controls and each transmittal to foreign governments may be made only with prior approval of NOL.		
11. SUPPLEMENTARY NOTES		12. SPONSORING MILITARY ACTIVITY
13. ABSTRACT		
<p>New results are presented for inviscid, supersonic and hypersonic blunt-body flow fields obtained with a numerical time-dependent method patterned after that of Moretti and Abbett. In addition, important comments are made with regard to the physical and numerical nature of the method. Specifically, numerical results are presented for two-dimensional and axisymmetric parabolic and cubic blunt bodies as well as blunted wedges and cones; these results are presented for zero degrees angle of attack and for a calorically perfect gas with $\gamma = 1.4$. The numerical results are compared with other existing theoretical and experimental data. Also, the effects of initial conditions and boundary conditions are systematically examined with regard to the convergence of the time-dependent numerical solutions, and the point is made that the initial conditions can not be completely arbitrary. Finally, in order to learn more about the performance of the time-dependent method, a numerical experiment is conducted to examine the unsteady propagation and region of influence of a slight pressure disturbance introduced at a point on the surface of a blunt body.</p>		

DD FORM 1473 (PAGE 1)
1 NOV 65
S/N 0101-807-6801

UNCLASSIFIED
Security Classification

14 KEY WORDS	LINK A		LINK B		LINK C	
	ROLE	WT	ROLE	WT	ROLE	WT
1. Blunt Body 2. Supersonic 3. Hypersonic 4. Inviscid Flow 5. Time-dependent 6. Numerical Solutions						